Radiation Sensing Using

Chalcogenide Glass Materials

by

Ankitha Chandran

A Thesis Presented in Partial Fulfilment
of the Requirements for the Degree
Master of Science

Approved November 2012 by the
Graduate Supervisory Committee:

Michael N Kozicki, Chair
Hugh Barnaby
Keith Holbert

ARIZONA STATE UNIVERSITY

December 2012

ABSTRACT

The dissolution of metal layers such as silver into chalcogenide glass layers such as germanium selenide changes the resistivity of the metal and chalcogenide films by a great extent. It is known that the incorporation of the metal can be achieved by ultra violet light exposure or thermal processes. In this work, the use of metal dissolution by exposure to gamma radiation has been explored for radiation sensor applications.

Test structures were designed and a process flow was developed for prototype sensor fabrication. The test structures were designed such that sensitivity to radiation could be studied. The focus is on the effect of gamma rays as well as ultra violet light on silver dissolution in germanium selenide ($Ge_{30}Se_{70}$) chalcogenide glass. Ultra violet radiation testing was used prior to gamma exposure to assess the basic mechanism. The test structures were electrically characterized prior to and post irradiation to assess resistance change due to metal dissolution. A change in resistance was observed post irradiation and was found to be dependent on the radiation dose. The structures were also characterized using atomic force microscopy and roughness measurements were made prior to and post irradiation.

A change in roughness of the silver films on $Ge_{30}Se_{70}$ was observed following exposure. This indicated the loss of continuity of the film which causes the increase in silver film resistance following irradiation. Recovery of initial resistance in the structures was also observed after the radiation stress was

removed. This recovery was explained with photo-stimulated deposition of silver from the chalcogenide at room temperature confirmed with the re-appearance of silver dendrites on the chalcogenide surface. The results demonstrate that it is possible to use the metal dissolution effect in radiation sensing applications.

ACKNOWLEDGEMENTS

I owe my deepest gratitude to Dr Michael N Kozicki whose encouragement guidance and support from the beginning developed my understanding of the subject.

I am grateful to my committee members Dr. Hugh Barnaby and Dr. Keith Holbert for their interest in my work and their support throughout the project.

I would like to thank Dr Dieter Schroder for his teaching developed my interest in semiconductor devices.

I would like to sincerely thank center for solid state electronics research, Arizona state university and their staff for guiding me with my thesis work and their support. I would like to show my gratitude towards the center for Leroy erying center for solid state science for their lab support. I would like to thank Dr Michael Goryll for his time and use of his lab facility. I would like to thank Dr Maria Mitkova and her students at Boise State University for their help and support in carrying out the material analysis at their facility.

My sincere thanks goes to my team members and my seniors whose early assistance served crucial in building my background . In particular I would like to thank Dr Yago Gonzalez Velo for his guidance and help throughout my course of work.

Lastly, I would like to thank my family and friends who always stood by my endeavors.

TABLE OF CONTENTS

Page

Page

Page

LIST OF TABLES

Table Page

LIST OF FIGURES

Figure Page

Figure Page

Figure Page

LIST OF ABBREVIATIONS

AFM	Atomic Force Microscopy
ChG	Chalcogenide
EDS	Energy dispersive spectroscopy
PMC	Programmable metallization cell
SEM	Scanning electron microscopy
SPM	Scanning probe microscopy
TEM	Transmission electron microscopy
UV	Ultra violet
RTA	Room temperature annealing
HMDS	Hexamethyldisilazane

1 Introduction

1.1 Radiation sensors

Radiation sensors are used to detect and quantify radiation. Radiation sensors and detectors find applications various fields but mainly they are used to identify the level of contamination, identify the radioactive material, personal dosimeters and in medical diagnostics and therapy [1]. It is important that we have radiation sensors that are sensitive with a high degree of resolution and that are cost effective.

Ionizing radiation is capable of creating charges in the material. The energy of the radiation is high enough to ionize molecules and penetrate through the material itself. This range above U.V light consists of high frequency radiation such as α, β, γ or cosmic rays.Many of the radiation sensors based on ionization are used to sense the radiation itself (detect and quantify radiation from sources such as X-rays and from nuclear sources (α, β, and γ radiation). Higher the frequency, higher is the photon energy. This results in the electrons being removed from the atoms [2].

There are three basic types of radiation sensors namely the ionizing sensors, scintillation sensors and the semiconductor radiation sensors. Ionizing sensors consist of chamber filled with gas with an inner lining of electrodes. The gas could be air or gases like krypton or xenon depending on the application. When radiation enters the chamber, it ionizes the gas molecules and current begins to flow. The amount of current is indicative of the radiation dose rate. In the case of

scintillation sensors crystals such sodium iodide are used so that incident radiation is converted into light. This light is then multiplied using a photo multiplier tube. These sensors use high efficiency crystals and are highly sensitive to radiation especially at high doses. Semiconductor radiation sensors convert the incident radiation directly into light. The radiation can cause charges to move across the band gap of the semiconductor. Higher band gap materials and thicker materials are preferred for higher ionizing radiations. These sensors have very good energy resolution but the cost is high compared to the other options available in the market.

In the case of both ionization chamber and scintillation sensors, the amplification circuitry may be complex. In the case of semiconductor sensors at low levels of radiation, the current produced becomes comparable to the background or the dark current. This results in their use only at cryogenic temperatures. It is keeping these issues in mind that a new sensor should be developed. Any sensor must have a well defined set of the following parameters. These are sensitivity, range and precision [3].

The sensitivity of the sensor is defined as the slope of the output characteristic curve more generally, the minimum input of physical parameter that will create a detectable output change. The range is defined as the maximum and minimum value of the applied parameters that can be measured by the sensor. The concept of precision refers to the degree of reproducibility of a measurement. If exactly the same value were measured a number of times, an ideal sensor would output

exactly the same value every time as the first irradiation indicating good reproducibility.

1.2 Chalcogenide glass materials

The group 16 elements of the periodic table are called chalcogens. Oxygen is a part of this group but usually the term chalcogenide is usually reserved for sulphide, selenide and telluride. The chalcogens combine with elements like germanium to form a base glass [4, 5]. Copper or silver is dissolved into this base glass [6, 7]. This dissolution decreases the resistivity of the chalcogenide (ChG) material. ChG glasses are used as solid electrolytes. These electrolytes are super ionic in nature with a metal rich phase that is ionic and a good electron conductor [7].

1.2.1 Chalcogenide based non-volatile memories

Programmable metallization cell (PMC) memory which uses solid state electrochemistry is a promising candidate for future solid state memory. ChG glasses are used as the solid electrolyte in PMC devices [8]. The ability of ChG materials to transport ions favours their use in the fabrication of PMC devices. Silver/copper can be diffused into glasses (ChG) with the use of UV light, a process called photo diffusion. The PMC device consists of a two terminal structure – an inert bottom electrode, the solid electrolyte and the oxidizable top electrode. These electrodes are separated by a dielectric medium. Vias or holes through the dielectric allow the solid electrolyte to make a contact with the electrodes. The active area of the device depends on the diameter of these vias or

holes [9]. The bottom electrode is an electrochemically inert material such as platinum, tungsten, nickel etc. Silicon dioxide is commonly used as the dielectric material. The solid electrolyte consists of ChG glasses that are doped (photo diffused) with silver. The silver combines with the chalcogenide to form a solid electrolyte of high resistivity but with high silver ion mobility.

Information is stored in the device by bringing about electrical changes causing oxidation of the silver metal and reduction of the silver ions into the electrolyte. Silver gets deposited on the cathode resulting in a change in resistance between the two electrodes at a very low bias- few hundred mV. A reverse bias can reverse the electro deposition process increasing the resistance of the device erasing the device. The process of writing and erasing the devices takes place in the order of ns and for currents in the range of μA. The information is stored in the form of metal atom electro deposition instead of charge storage which results in better retention.

A double sweep is performed on the PMC device as illustrated in figure1. During the forward sweep we see high resistance across the electrolyte (A), the silver ions get oxidized with a positive voltage and silver ions now move under the influence of the electric field(B). The silver ions get reduced at the cathode end and start getting deposited forming a filament extending from the cathode to the anode through the doped electrolyte (C). When a metallic filament connection is established between the anode and the cathode the current increases and reaches compliance level (D), the voltage at which this takes place is known as the set

voltage. This is the low on state resistance of the device and when swept in the reverse direction, the silver from the filament forms silver ions and the link between the anode and cathode is not complete anymore resulting in high value of resistance known as off state resistance (E). The voltage at which the device is turned off and the resistance increases is called the reset voltage.

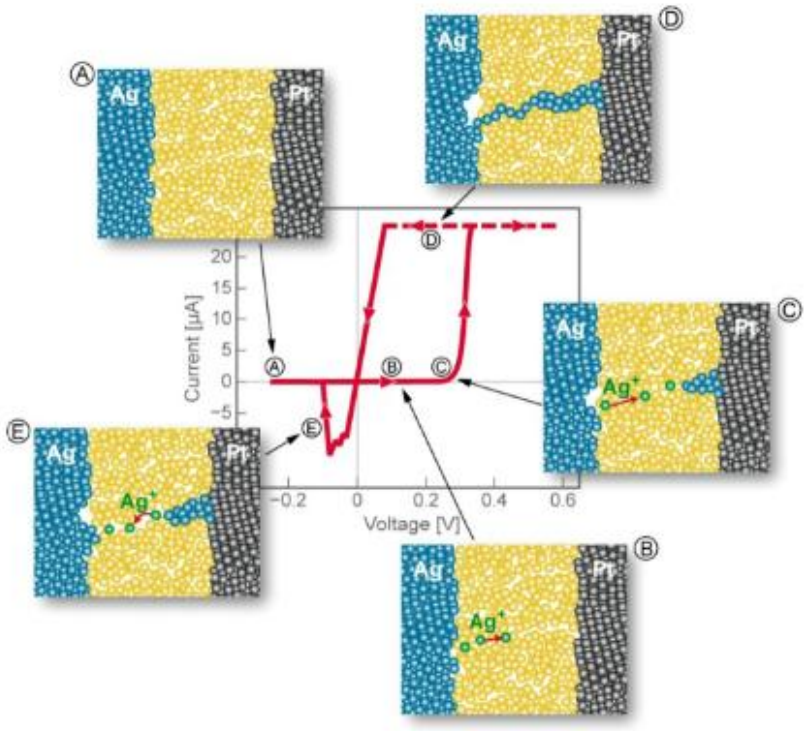

Figure 1: Double sweep being performed on a PMC device describing the different stages of growth and dissolution of the filament [10].

The resistivity of the electro deposit is many times of order lower than that of the electrolyte; hence once it is formed current increases until the compliance level is reached in the device. This is the low on state resistance of the device. When reverse bias is applied the electro deposit dissolves and the metal moves back to

its source. Once the electro deposit has been dissolved the device is at high off state resistance.

1.3 Resistive radiation sensor

The incorporation of silver into chalcogenide films changes the resistivity of the chalcogenide glass and the silver layer above [11]. This incorporation has been noticed with UV light (photo-diffusion). Silver has a high mobility in ChG and this diffusion takes place at room temperature. The incorporation can be enhanced using photo-diffusion. The change in resistance of the silver film above the chalcogenide film with gamma and UV radiation has been studied within the scope of this work. This study was carried out on undoped (no photo-diffused silver) ChG ($Ge_{30}Se_{70}$) films with silver films on top. Test structures are designed such that we can study the incorporation of silver into chalcogenide films upon exposure to radiation. The change in resistance brought about upon irradiation can be put to use in a detector/ sensor.

2. Fabrication of test structures

2.1 Sensor principle

The test structures were designed with the following principle in mind. A low resistance (continuous) silver film prior to irradiation and a high resistance (discontinuous) silver film post irradiation as shown in figure 2.

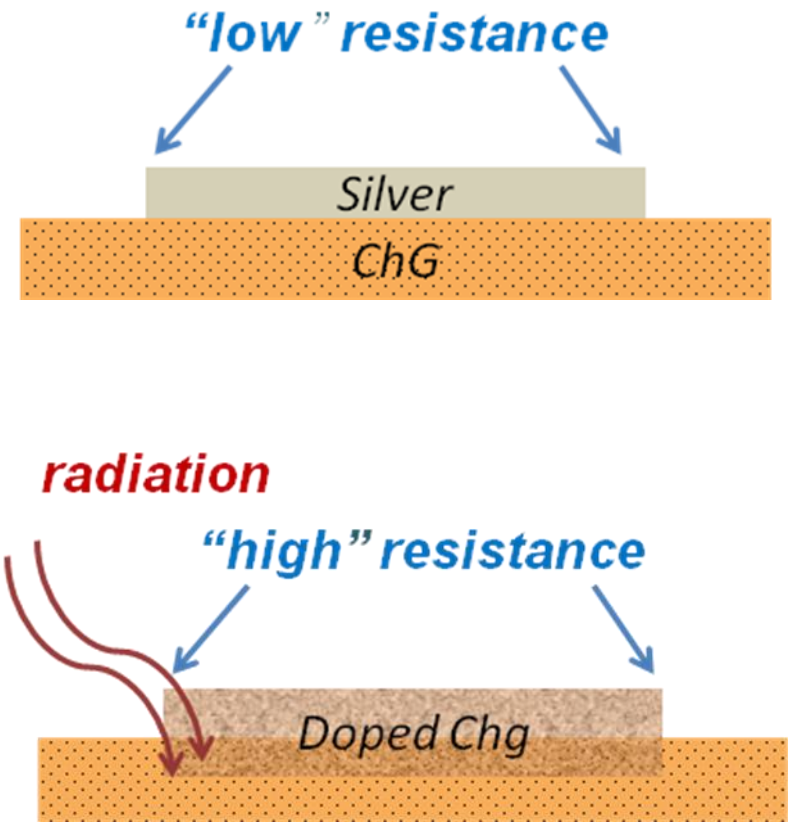

Figure 2: Principle of ChG based sensor operation

These structures are designed such that after processing we are measuring the resistance of a patterned silver pad on blanket Ge30Se70 which corresponds to a low resistance state compared to a high resistance state post irradiation.

2.2 Mask design of test structures

A mask was designed using AUTOCAD software to process test structures. The mask was designed considering that positive photo resists would be used; these will be dark field masks. Nickel is used as the electrode material on top of the silver pad. It is used as because it is inert in nature and can be easily evaporated at moderate temperatures. Silver cannot be probed directly as silver on top of Ge30S70 can diffuse at room temperature or when exposed to radiation. There are two masks required for the processing of these test structures.

2.2.1 Mask 1- Silver pad mask

Mask 1 is designed to put down patterned silver on blanket germanium selenide (30:70). It consists of rectangular pads such that there will be nickel fingers deposited on top of the silver. The layout of these pads is as shown in figure 3. The corners of the pads have been rounded off to avoid high electric field at that the corners. The radius is 2μm and this is consistent throughout the mask design for all features with corners.

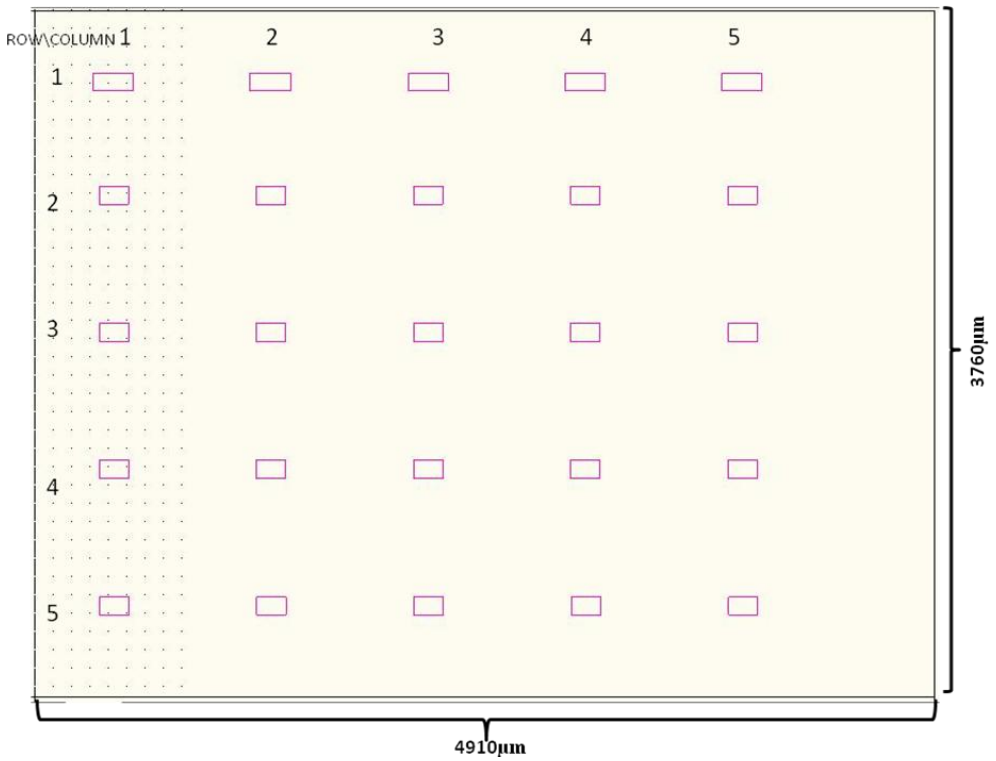

Figure 3: Layout of mask 1-silver pad mask

The pink rectangular pad is the pattern for putting silver on the Ge30Se70. These have been spaced apart such that we have enough room for depositing electrode material (Ni) on top. The breadth of each rectangle is 100µm and is the same for all 16 structures on the die. The length of the pads in row 1 is 220µm and the pads in rows 2-5 is 160µm.

2.2.2 Mask 2- Nickel electrode mask

Mask 2 is designed to put down the nickel electrode on top of the thin patterned silver film. There are two different types of structures on the same die depending on how the nickel electrode is patterned. The layout of the mask is as shown in the figure 4.

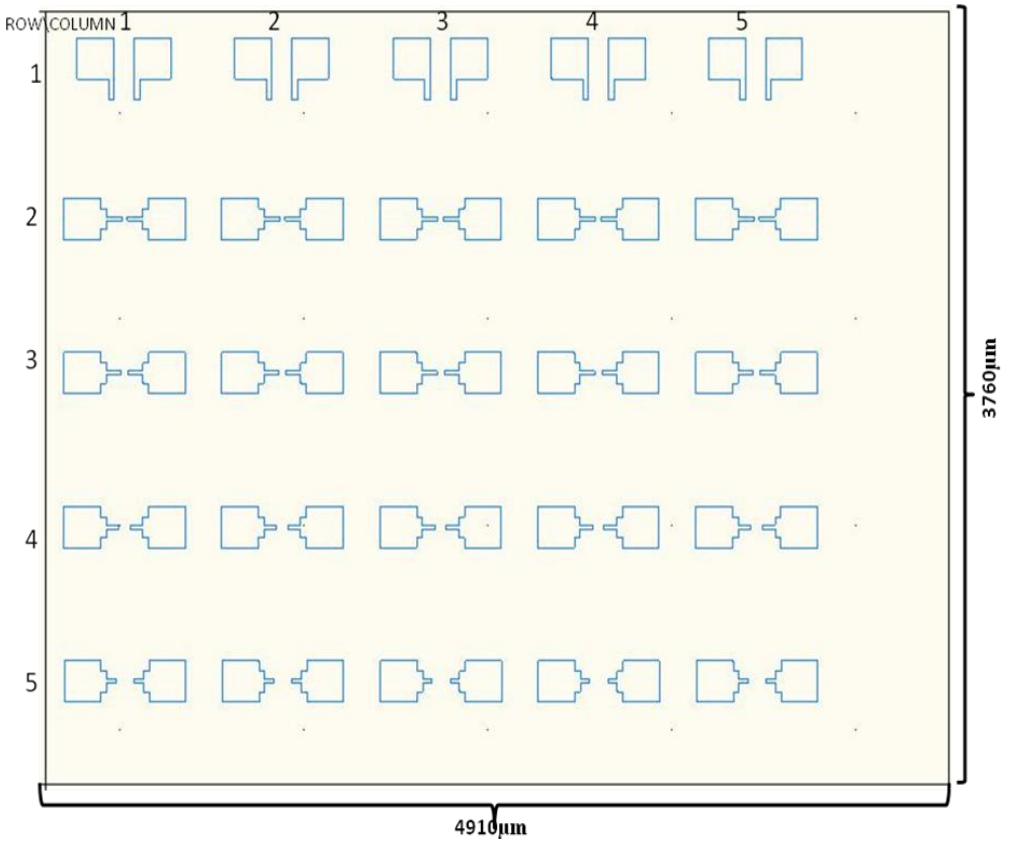

Figure 4: Layout of mask 2- nickel electrode mask

There are two different structures on the mask- type A (with the electrode fingers parallel to one another)and type B (with the electrode fingers along the same line facing one another).There are five type A structures along the first row, the spacing between the fingers is fixed at 100 µm. The rows from second to fifth row are type B structures. The spacing between the fingers increases row wise (30, 40, 60, 100µm).

2.2.3 Type A and type B structures

Mask 1 and mask 2 results in the design of two types of structures. The dimensions of both the structures have been labelled in figure 5 and figure 6

respectively. The finger spacing for type B structure is 30, 40, 70 and 110 microns. In the case of type A structure, we have fingers running parallel with a constant spacing between them (110µm). Type B structures have fingers facing each other with variable spacing between them.

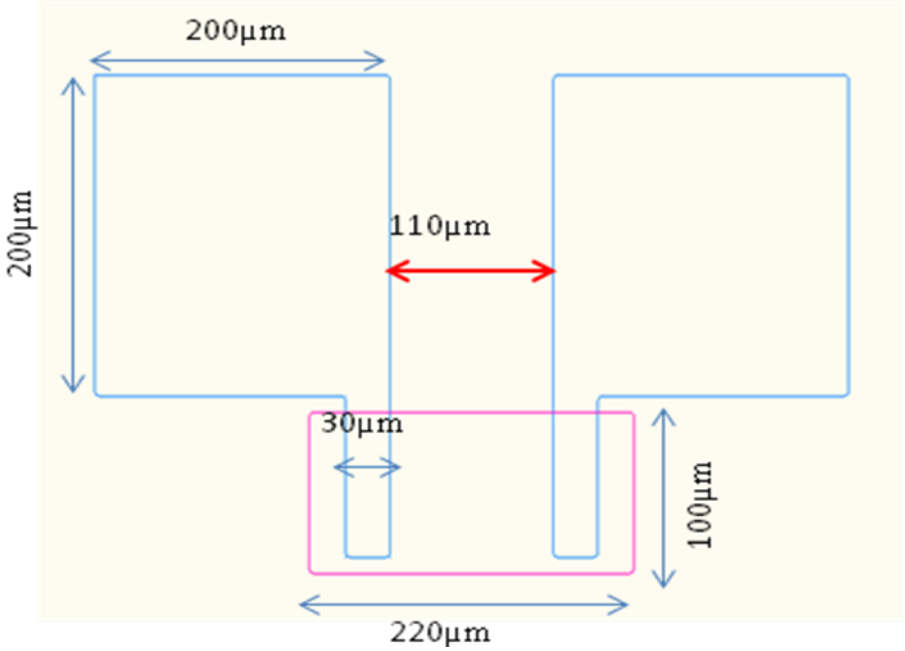

Figure 5: Dimensions of type A structure

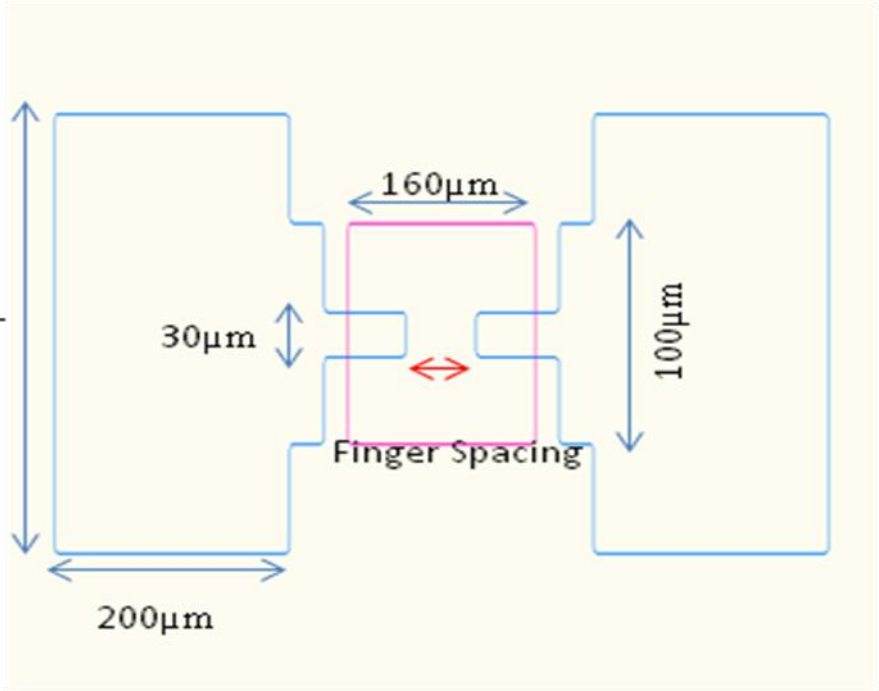

Figure 6: Dimensions of type B structure

2.3 Process flow for the test structures

The processing of these structures was carried out in the clean room at CSSER and ERC 139 at Arizona State University. The steps used to manufacture the devices are:

Clean room Conditions: Temperature = 70.6˚F; Humidity = 42 %

Step1: 80 nm of silicon dioxide is deposited on Si substrate (e beam deposition). It is deposited as a blanket and not patterned. The details of the deposition are as follows:

Tool: Torrvac e-beam evaporator

Base Pressure: 3e-6 Torr

Deposition rate: 1.3A˚/s

Beam current: 20-30 mA

Step2: 60 nm of ChG $Ge_{30}Se_{70}$ deposited over the SiO_2 (thermal evaporator).It is deposited as a blanket and not patterned. The details of the deposition are as follows:

Tool: Edwards 306 A / Cressington 308

Base Pressure: 3e-6 Torr

Deposition rate: 1A˚/s

Beam current: 40-45 Amperes

Step3: 34 nm of silver patterned (thermal evaporator).The silver is patterned using silver pad mask.

HMDS (hexamethyldisilazane, adhesion promoter) and AZ 3312 (positive photoresist) is spun at 3500rpm for 30 seconds on the sample. It is then soft baked on a hot plate for 60 seconds at 100˚C.

It is then exposed using OAI 808 Aligner for time = 12 seconds, and intensity of 6.9mW/cm^2. The sample is then developed in 300 MIF developer for 35 seconds.

Sample is then loaded into the Cressington 308 thermal evaporator or Edwards XXX thermal evaporator for silver deposition details of which are as follows:

Tool: Edwards 306 A / Cressington 308

Base Pressure: 3e-6 Torr

Deposition rate: 0.7A˚/s

Beam current: 50-60 A

Lift-off in acetone.

Step4: 60 nm of nickel patterned (e beam evaporation).The silver is patterned using nickel electrode mask.

HMDS (hexamethyldisilazane, adhesion promoter) and AZ 3312 (positive photoresist) is spun at 3500rpm for 30 seconds on the sample. It is then soft baked on a hot plate for 60 seconds at 100˚C.

It is then exposed using OAI Aligner808 for time =12 seconds, and intensity of 6.9mW/cm^2.The sample is then developed in 300 MIF developer for 35 seconds.

Sample is then loaded into the tool Torrvac for nickel deposition details of which are as follows:

Tool: Torrvac e-beam evaporator

Base Pressure: 3e-6 Torr

Deposition rate: 1A˚/s

Beam current: 60-70 mA

Lift-off is in acetone.

2.4 Cross-section of type A and type B structure

The cross-sections of type A and type B structure have been shown in the figure 7 and 8 respectively.

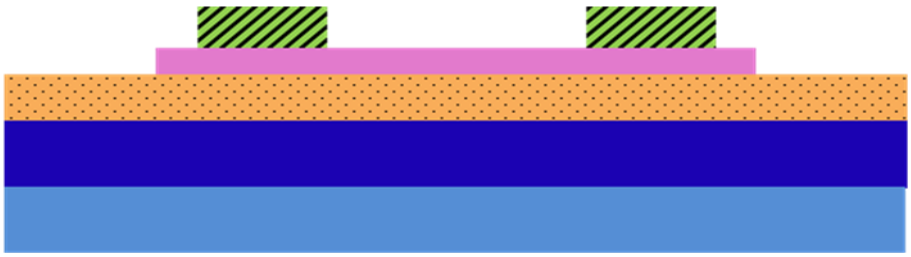

Figure 7 : Cross- section of type A structure

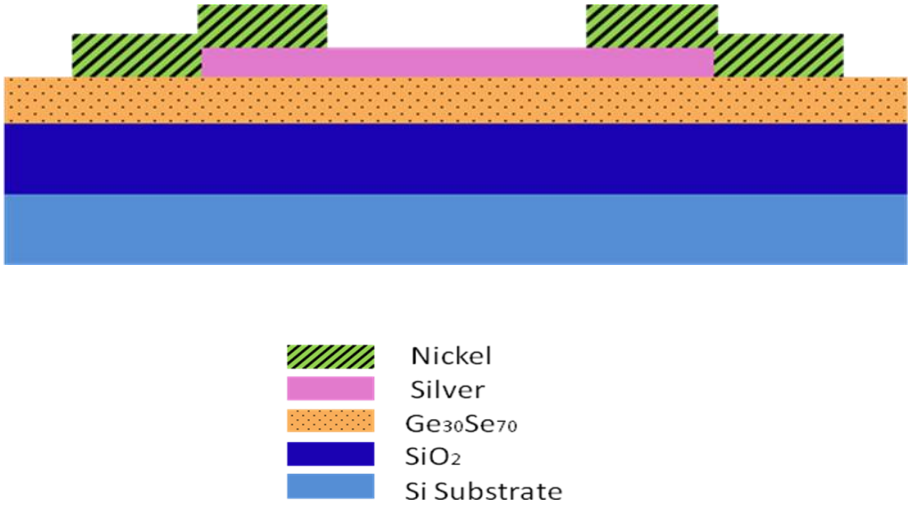

Figure 8: Cross-section of type B structure

Layer	**Thickness**
Nickel	60 nm
Silver	40 nm
$Ge_{30}Se_{70}$	60 nm
SiO_2	120 nm
Si substrate	525±25µm

Table 1: Thickness of layers deposited for the test structure

2.5 Optical images of type A and type B structures

Optical images of the structures were taken using the Axiophot (high resolution optical microscope). Images of good resolution were obtained using the same.

Figure 9 and 10 are the images of type A and type B structures. Images are taken soon after the structures are manufactured and they help in early analysis of the test structures. We could see on some test structures that there was silver diffusion taking place at room temperature itself without being exposed to any irradiation. It was noticed that there appeared a halo of diffused silver around the patterned silver indicating that some diffusion of silver into the ChG was taking place at room temperature possibly due to the processing steps involved.

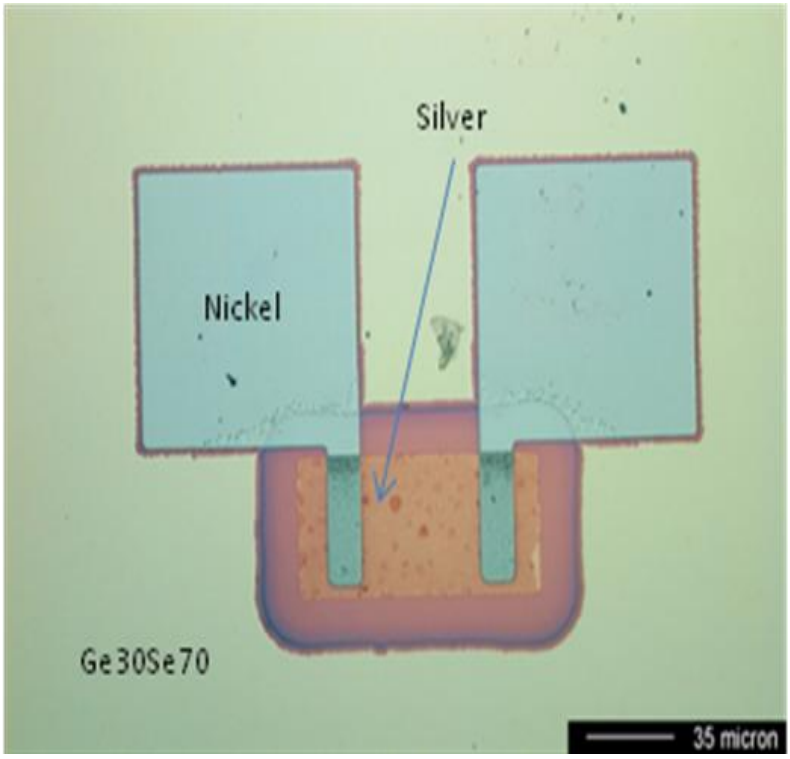

Figure 9: Optical image of type A structure

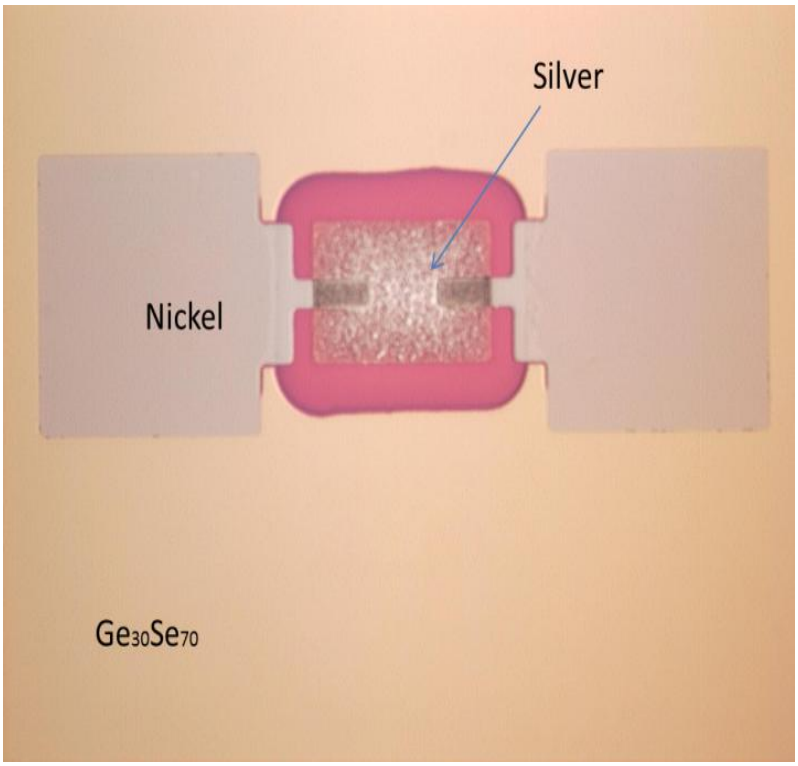

Figure 10: Optical image of type B structure

3 Electrical characterization of test structures

Electrical characterization performed on the test structures was current voltage characterization. These characteristics were measured with a computer controlled Agilent 4156C semiconductor parameter analyzer. The substrate of the wafer was left floating during the measurement. These measurements were conducted on a probe station with guarded co-axial cables. The experiment was carried out with minimal ambient light and there was no microscope light on the structures during the measurement. The structures were always stored in a black box (away from light). These measures were taken as the silver is sensitive to light and to ensure there is minimal change in the test structure due to the experimental set-up.

3.1 Current voltage characteristics of test structures prior to irradiation

The structures were fabricated such that they have high conductivity (low resistivity), because the thin layer of silver deposited on top of the ChG between the electrodes provide a current path (low resistance). The voltage was swept from 0V to 0.1V. A low value of voltage of 0.1 V was chosen to ensure there was no change brought about due to high bias. Silver moves at higher bias voltages and this can account for the resistance value being measured.The experiment was conducted on three dies: one used as a control, one used to get the behaviour at low dose steps under 200krad and the third sample used for exposure to higher dose, without small dose steps.The characteristics of type A and type B(40 and 110 μm) structures was studied.

3.1.1 Pre-irradiation characteristics of type A structure -110µm spacing

On figure 11, current voltage characteristics of three die have been plotted. Die 1, plotted in black has currents measured on 5 different type A structures. Die 2, plotted in red has currents measured on 5 different type A structures. Die 3, plotted in green has currents measured on 5 different type A structures.

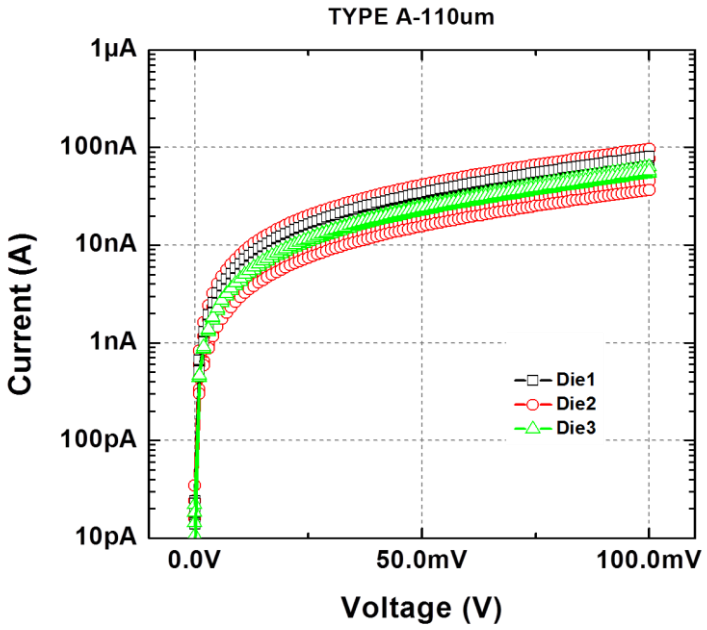

Figure 11: Current voltage characteristics obtained on type A structures

It was seen that the pre-radiation current flowing through these devices is close to 100nA. The currents were all in hundreds of nA range for voltages higher than 50mV, with values obtained on different similar devices on one die repeatable. A high pre-irradiation resistance level was noticed.

3.1.2 Pre-radiation characteristics of type B structure with 110µm and 40µm between electrodes

The pre-radiation characteristics of type B structures with 110 and 40 µm spacing have been plotted in figure 12.

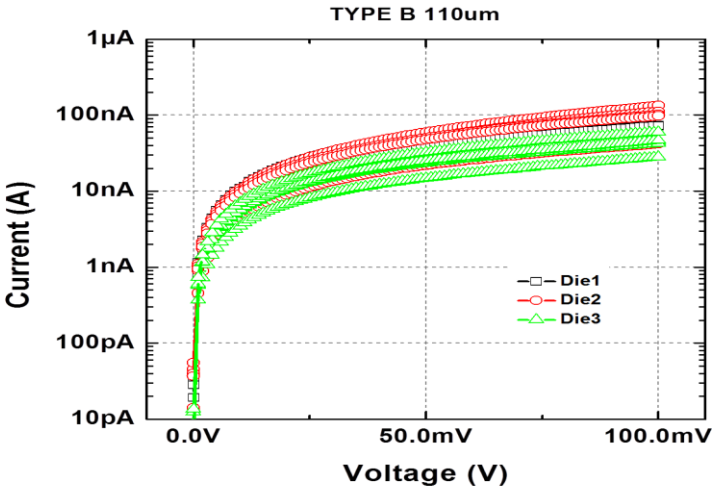

(a)

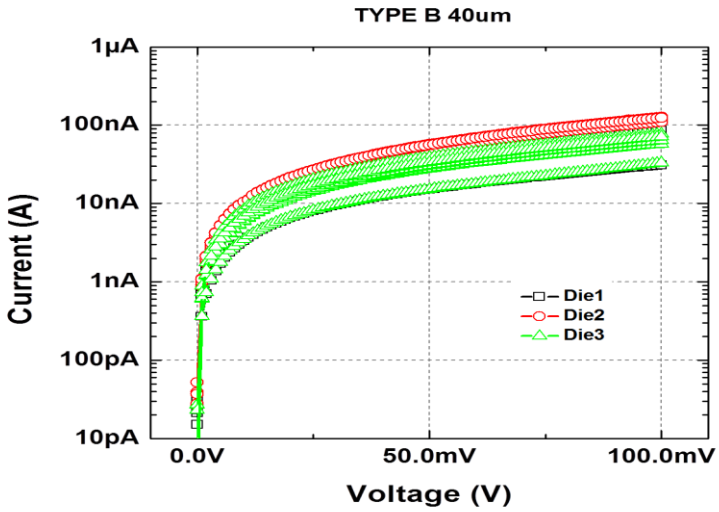

(b)

Figure 12: Current voltage characteristics for type B structures 110µm (a) and 40µm (b)

The currents measured on these structures were comparable to the currents measured on structures of type A with the parallel electrodes. Measurements were carried out on 5 structures of two different finger spacing- 110 µ and 40µm.It was seen that for both finger spacing, the range of current value is comparable (no clear scaling of resistance with length). The current level of both types of devices (type A and type B) was also comparable. The measurements are repeatable on different dies and for the different structures on the same die with one order of spread in magnitude. This spread may be due to non uniformities from processing parameters such as thickness on different dies as well on the same die.Also , there is diffusion of silver taking place at room temperature.

3.2 Irradiation of test structures

The test structures were exposed to gamma rays of a cobalt 60 source (Gamma cell 220) at the radiation damage lab (Arizona State University). The exposure was carried out without any bias applied on the devices. The test structures were taped on a breadboard with double-sided tape. The measurements were carried out on a probe station located in different lab. The structures were irradiated and then taken to this lab to perform the measurements. These usually lasted 15-20 minutes for one die.

The dose-rate during this experiment is approximately 10.5 rad/s. The experiment was conducted on three dies: one used as a control, one used to get the behaviour at low dose steps under 200krad and the third sample used for exposure to higher dose, without small dose steps.

The schedule of the radiation exposure as well as of the different room temperature measurements has been provided in the following tables. Annealing refers to the change in resistance observed when these dies were left at room temperature in a black box after the irradiation was stopped.

Irradiation Time Step (hh:min:sec)	**Irradiation Time Step (sec)**	**Dose step (Rad)**	**Total Irradiation Time**	**Total Dose (Rad)**
01:58:00	7080	74340	7080	**74340**
01:59:00	7140	74970	14220	**149310**
03:31:00	12660	132930	26880	**282240**
15:30:00	55800	585900	82680	**868140**
07:07:00	25620	269010	108300	**1137150**
14:39:00	52740	553770	161040	**1690920**
07:45:00	27900	292950	188940	**1983870**
14:45:00	53100	557550	242040	**2541420**

Table 2: Exposure schedule of the experiment for die 2

Irradiation Time Step (hh:min:sec)	**Irradiation Time Step (sec)**	**Dose step (Rad)**	**Total Irradiation Time**	**Total Dose (Rad)**
01:58:00	7080	74340		
00:24:00	1440	15120		
01:59:00	7140	74970		
00:20:00	1200	12600		
03:31:00	12660	132930		
00:26:00	1560	16380		
15:30:00	55800	585900	86880	**912240**
07:07:00	25620	269010	112500	**1181250**
14:39:00	52740	553770	165240	**1735020**
07:45:00	27900	292950	193140	**2027970**
14:45:00	53100	557550	246240	**2585520**

Table 3: Exposure schedule of the experiment for die 3

	Date	**Step Duration**	**Total Time s**
RTA0	5/4/2012 9:40	25:38:00	92280
RTA1	5/6/2012 12:05	52:25:00	188700
RTA2	5/7/2012 12:22	24:17:00	87420
RTA3	5/10/2012 15:44	75:22:00	271320

Table 4: Approximated times at which the irradiated devices have been controlled

3.2.1 Evolution of the current of lateral test structures after exposure to Co60 γ-rays and after a period at room temperature annealing

The electrical characterization was performed less than ten minutes after the end of the exposure. Electrical characterizations performed on these test structures are current-voltage characteristics measured with a computer controlled Agilent 4156C semiconductor parameter analyzer. Voltage was swept from 0V to 100mV. The values of current reported on the variation of current as a function of dose and as a function of time are the mean values of the currents measured at a voltage of 50mV.

3.2.1.1 Evolution of current as a function of dose for type A structure

The evolution of current as a function of dose is shown in figure 13 for type A structures. In black are represented the control devices, in red are represented devices of type A from sample II on which current are measured for low total irradiated dose steps at the beginning, in green are represented devices of type A from sample III. The current presented here are for 5 devices of type A for each of the three dies tested.

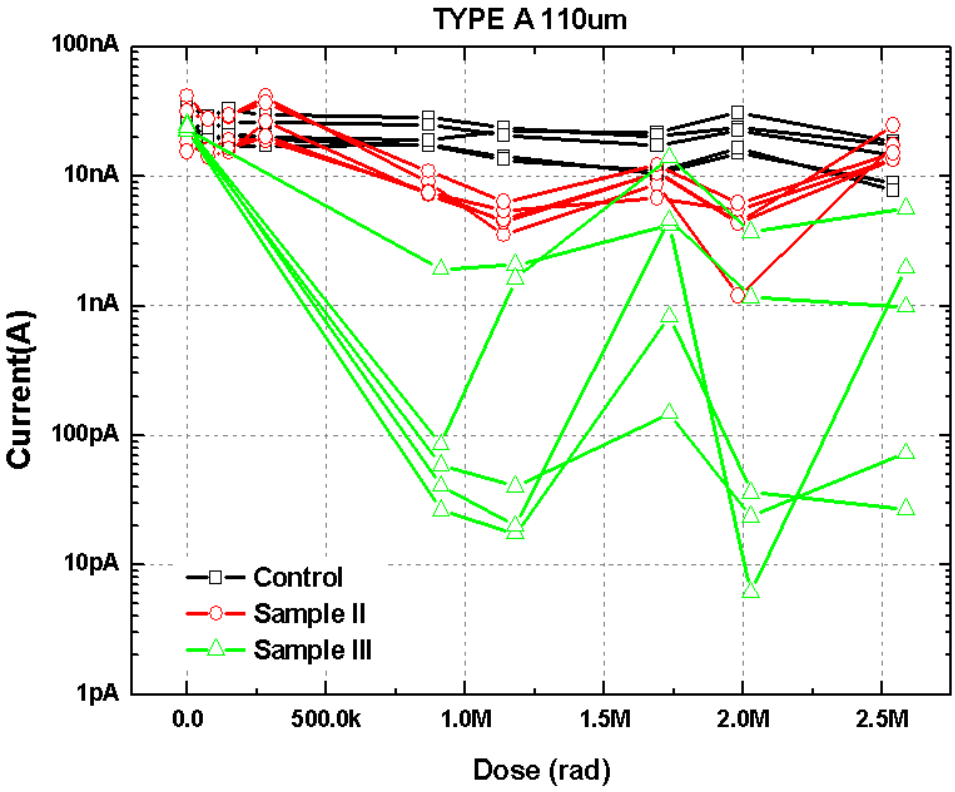

Figure 13: Evolution of current as a function of dose for type A structures

3.2.1.2 Current variation as a function of time for type A structure

The current evolution as a function of time is shown in figure 13 for type A structure. In black are represented the control devices, in red are represented devices of type A from sample II on which current are measured for low total irradiated dose steps at the beginning; in green are represented devices of type A from sample III. The first 250k seconds are the evolution of the current while devices are exposed to gamma ray (highlighted with a pink area), while the room thermal annealing period goes from 250k seconds to 1M seconds

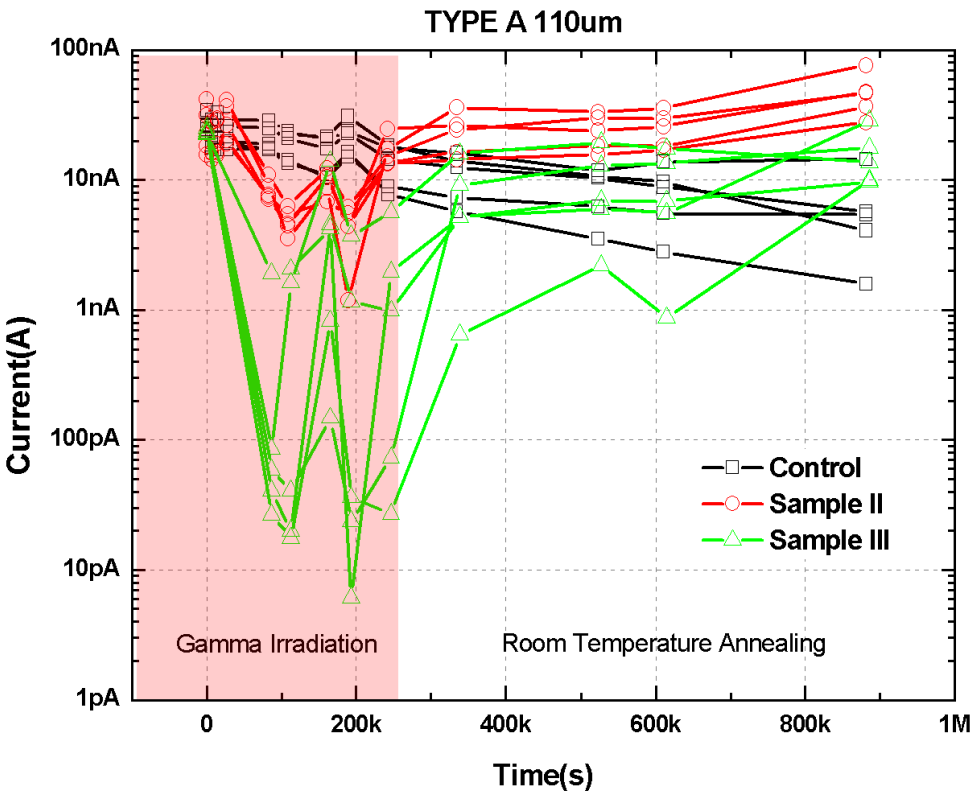

Figure 14: Evolution of current as a function of time for type A structures

On figure 14, the evolution of the current as a function of dose (figure 13) is plotted for the control structures (black curve), devices irradiated to 2.54 Mrad

and the left at room temperature (red curve), and also structures irradiated to approximately 2.58 Mrad (green curve) and left at room temperature. The shaded region of the evolution of a current as a function of time curve represent the gamma irradiation part of the experiment when the dies were kept in the irradiation chamber and taken out at intervals for electrical characterization.

The current level lowers with radiation dose. The magnitude of the current variation is different for devices on dies 2 and 3. This can be due to an impact of the several characterizations conducted on sample II at lower total doses, while sample III remains in the irradiator until 912krad.Current on the control devices comes down by 1 order of magnitude (black curve) during the whole experiment. Most of the variation is observed during the one week room thermal annealing period. The low total dose (on sample II), the current was constant after several small dose steps, but decrease at the same level as the initial and we see a decrease in current after longer periods of exposure Current level for die III (taken out after 912krad) is at a much lower level than that obtained on devices on die II. This suggests that devices have to be exposed to a certain value of dose (at once) to see the drop in current, or that performing repeated electrical characterization has an impact on the response of the devices. Current of devices irradiated decreases after exposure, but it can be seen on figure 13 that the current recovers to a level equivalent and higher to its initial level after 7 days of room temperature annealing.

3.2.2 Evolution of current as function dose and time for type B structures

3.2.2.1 Variation of current as a function of dose for type B-110 µm

The evolution of current as a function of dose is shown in figure 15 for type structure with 110µm spacing between the fingers: In black are represented the control devices, in red are represented devices from sample II, in green are represented devices of type B from sample III.

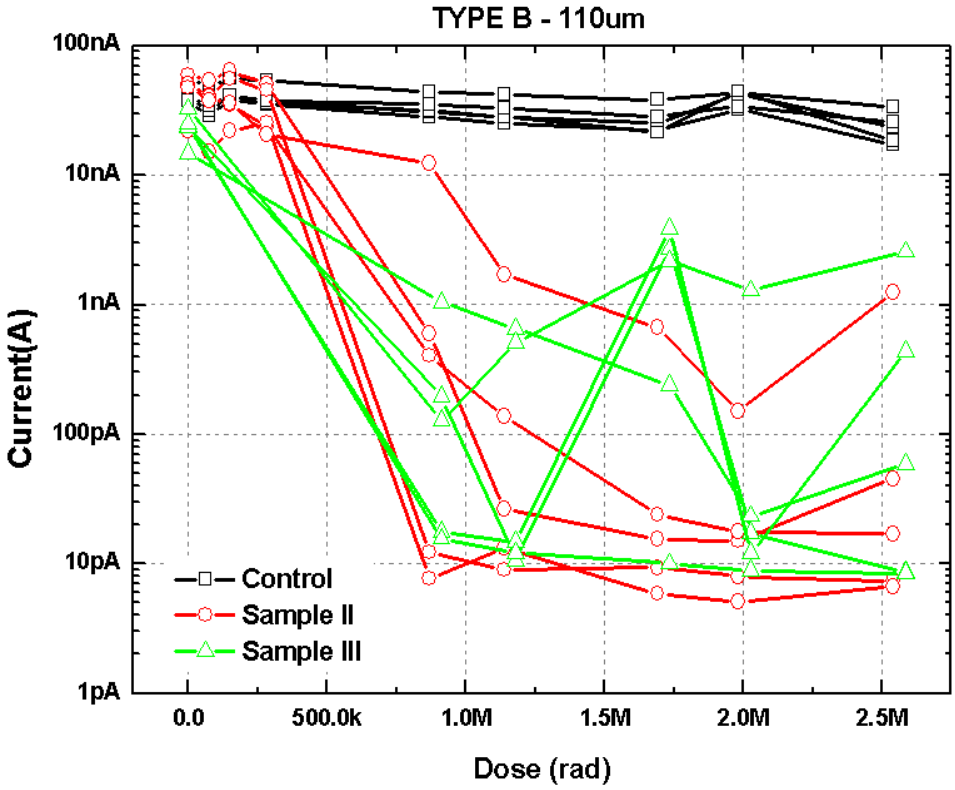

Figure 15: Evolution of current as a function of dose for devices of type B with 110um spacing between electrodes

On figure 15, the evolution of current as a function of dose for devices of type B 110um is plotted for control structures (black curve), structures irradiated to 2.54 Mrad and the left at room temperature (red curve), and also structures irradiated to

approximately 2.58 Mrad (green curve) and left at room temperature. The shaded region of the graph is the gamma irradiation part of the experiment when the dies were kept in the irradiation chamber and taken out at intervals for electrical characterization.

3.2.2.2 Variation of current as a function of time for Type B-110µm

The evolution of current as a function of time has been plotted for type B structure with 110µm spacing in figure 16. In black are represented the control structures, in red sample II which was taken out of the irradiation chamber more frequently than die 3, in green are the devices on sample III which was kept in the chamber for longer intervals.

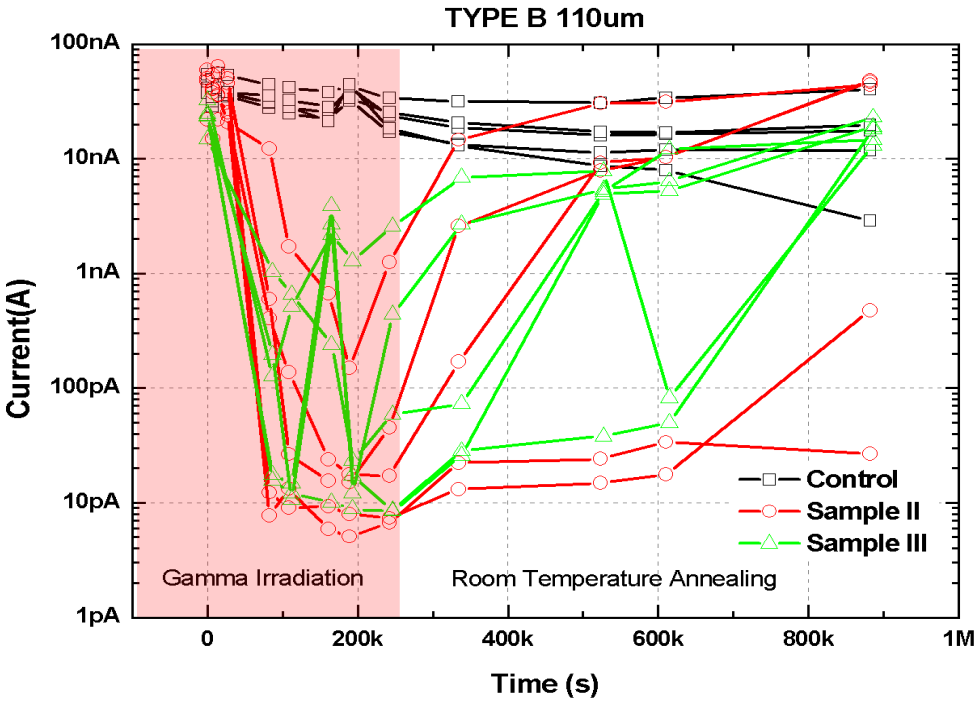

Figure 16: Evolution of current as a function of radiation dose for devices of type B 110um

It is observed from figure 14 and 15 that current decreases on the control structures (black curve) during the radiation exposure by one order of magnitude which might be the result of repeated measurements. Currents on structures from sample II do not decrease with dose for the lower dose steps (red curve on figure 7, fewer than 200 krad). At higher total doses, the current measured on these structures decreases by 2 and in some cases 3 orders of magnitude. Current on devices from sample III (green on figure 7 and figure 8) decreases with dose but increase back to the initial value when sample is left at room temperature for several days. Some devices exhibit a current after the room temperature annealing as high as their pre-irradiation current level.

3.2.2.3 Variation of current as a function of dose for type B- 40µm spacing

The evolution of current as a function of dose has been plotted for type B structure with 40µm spacing in figure 17. In black are represented the control devices, in red are represented devices from sample II, in green are represented devices of type B from sample III.

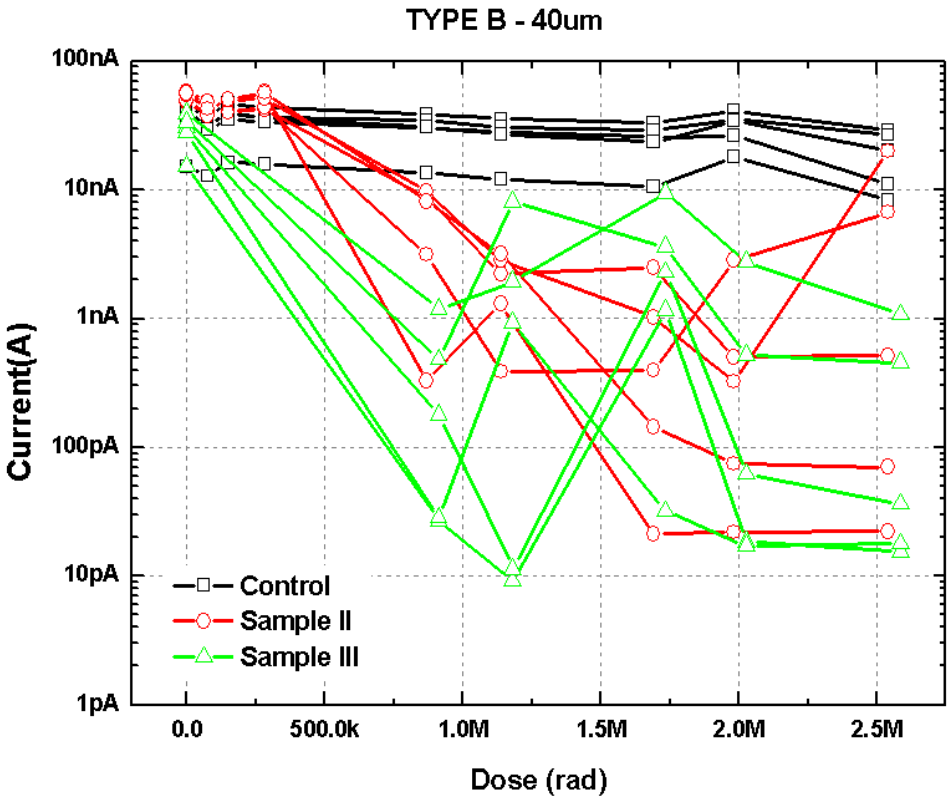

Figure 17: Evolution of current as a function of dose for devices of type B with 40um spacing between electrodes

3.2.2.4 Variation of current as a function of time

The evolution of current as a function of time has been plotted for type B structure with 40µm spacing in figure 18. In black are represented the control structures, in red sample II which was taken out of the irradiation chamber more frequently than die 3, in green are the structures on sample III which was kept in the chamber for longer intervals On figure 16 and 17, trends similar to the ones already observed for type A and type B structure (110µm) is obtained.

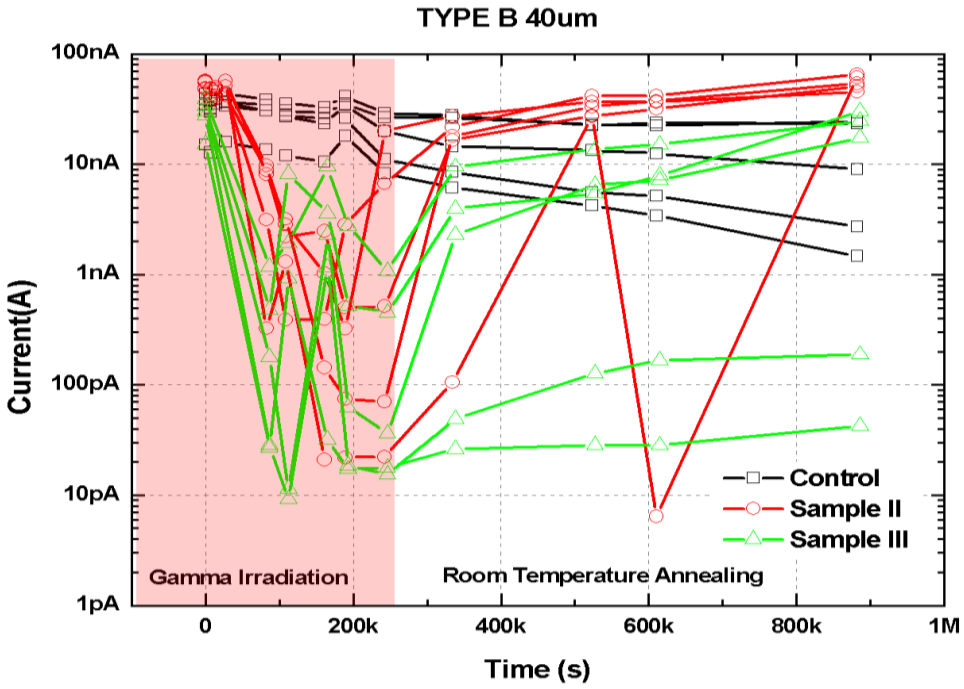

Figure 18: Evolution of current as a function of radiation dose for devices of type B 40um

The current does not decrease for the first dose steps on the structures from sample II (red curve) but decrease after a given dose. On several structures from sample II and sample, current increases are observed even after gamma ray exposure. The behaviour of structures of type B with spacing 110um and spacing 40um are very similar.

3.3 Evolution of the current with UV exposure and room temperature annealing

The type A test structures were exposed to UV light and measurements were made prior to and post exposure. The intensity of UV light used for the exposure is 1.9mW/cm^2 and the wavelength of light used is 324nm. This was carried out on

five type A structures on the same die. The details of the exposure steps have been listed in the table below.

Experiment Detail	DURATION (Minutes)	Duration Date	Date
PRE UV			05/10/12 4:55-5:30pm
UV EXPOSURE 1	60	05/11/12 9:15am-10:15am	05/11/12 10:25-10:55am
UV EXPOSURE 2	60	05/11/12 11:05am-12:05pm	05/11/12 12:18-12:36pm
UV EXPOSURE 3	75	05/11/12 12:45pm-2:00pm	05/11/12 2:13-2:30pm
UV EXPOSURE 4	80	05/11/12 2:40pm-4:00pm	05/11/12 4:13-4:34pm
ROOM TEMPERATURE ANNEALING 1	2440	05/11/12 4:35 pm- 05/14/12 9:15am	05/14/12 9:15-9:35am
RE UV EXPOSURE 1	330	05/14/12 10:00am-3:30pm	05/14/12 3:40-4:10pm
ROOM TEMPERATURE ANNEALING 2	1140	05/14/12 4:00pm-05/15/12 11:00am	05/15/12 11:00-11:30am
ROOM TEMPERATURE ANNEALING 3	1510	05/15/12 11:30am-05/17/12 12:40pm	05/17/12 12:40-1:00pm
ROOM TEMPERATURE ANNEALING 4	1420	05/17/12 1:00pm -05/21/12 12:40pm	05/21/12 12:40-1:00pm

Table 5: Schedule of U.V Exposure performed on type A structure

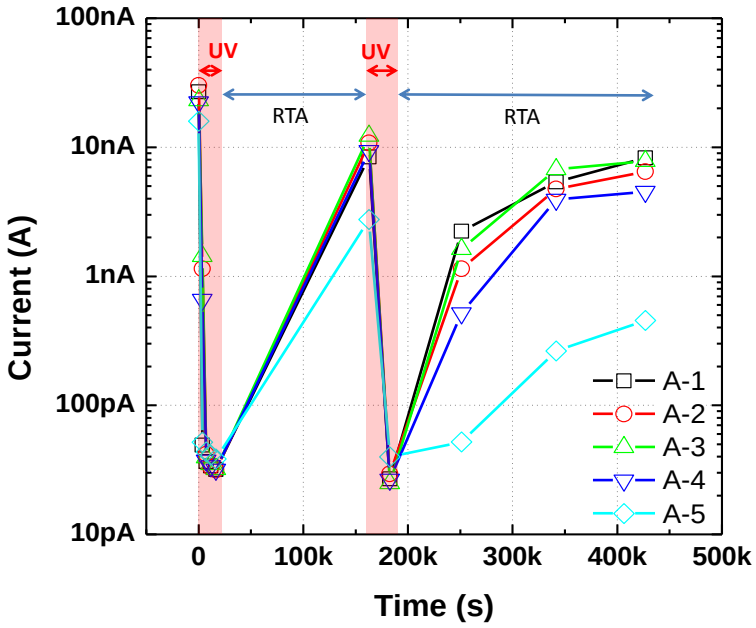

Figure 19: Evolution of current as a function of time with UV exposure and room temperature annealing.

The results were similar to that obtained from the gamma exposure. The shaded region in figure 19 indicates the UV exposure part of the experiment. The resistance increased upon exposure and went back to the initial level after they were left at room temperature. It followed the same trend when they were exposed to UV for the second time. The resistance increased on exposure and they recovered when left at room temperature. This was done to check if we could use the recovered test structures for testing purposes again and to see if they would continue to be sensitive to radiation.

3.4 Electrical results

The following observations were made during the course of the experiment- a high pre-irradiation resistance level, increase in resistance with radiation dose and recovery of resistance to pre-irradiation level post exposure at room temperature.

3.4.1 High pre-irradiation resistance level

A resistance value close to 1 MΩ was obtained prior to irradiation as opposed to resistance in the order of few tens of ohms. A metallic layer of silver corresponds to a sheet of very low resistivity with resistance in the order of few tens of ohms. This high value of resistance can be due to the processing steps that the structures undergo. Steps such as thermal evaporation of films can cause thermal diffusion of silver into the ChG. Agglomeration of thin silver films can also take place. Agglomeration results in reduction of inter-facial energy. This results in loss in continuity of the silver film above the ChG. Silver has high mobility in the ChG, this can cause some diffusion to take place at room temperature. All the three processes mentioned above result in the loss of a continuous silver film above the ChG resulting in a higher pre-irradiation resistance level.

3.4.2 Increased resistance with radiation dose

It was observed that there was change in resistance (increase) with radiation dose. There were three orders of change in the resistance level on radiation. This change was a function of the total irradiated dose. It was noticed that at smaller dose steps, there was no change in resistance of the test structure. The change was a function of the total irradiated dose. When radiation stress is applied there is

generation of electrons and holes in the ChG film. The generation of electrons and holes in the SiO_2 is not covered within the scope of this work. The Ag^+ ions combine with the electron and get neutralized.

$Ag^+ + e^- \rightarrow Ag$

$2Ag + Se \rightarrow Ag_2Se$

Ag_2Se clusters increase the density of the film [11,12] and as a result we have less continuous film of silver on top, this causes the drop in resistance when exposed to radiation.

3.4.3 Recovery of resistance at room temperature

Resistance recovers to a value close to the pre-irradiation resistance level when the irradiated test structures are kept at room temperature. This could be due to photo stimulated deposition [13] of silver on the surface at room temperature. The resistance measured is that of the silver film on top of the ChG. Silver ions migrate towards the surface resulting in a lowering of resistance. The force behind silver migration could be the photo excited electrons at the interface which attracts the excess silver ions in the glass by the electric field. There can also be photo-induced holes diffusing into the interior of the ChG glass and excess silver ions counter flow to the hole motion [14]. This results in silver being deposited at the surface of the film resulting in a lowering of resistance close to the pre-irradiation resistance level.

Recovery was also noticed in the case of some structures that stayed in the irradiator after being tested. The measurement time is long enough (1 hour in total for all die) for the recovery process to start. The structures do not stay at the low level of current and start recovering once they are placed back in the irradiator. In-situ testing can prove helpful in such situations.

3.5 Impact of Silver thickness on pre-irradiation resistance level

Two batches of structures were manufactured keeping the same processing conditions as described in section 2.3 of this study. The thickness of the silver layer was changed in the two batches. This had an impact on the initial resistance level of the structures. The thickness of the different layers used in the structures for the two different batches have been listed in table

Layer	**Thickness(Batch 1)**	**Thickness (Batch 2)**
Nickel	60 nm	60
Silver	40 nm	60
$Ge_{30}Se_{70}$	60 nm	90
SiO_2	120 nm	120
Si substrate	525$\pm$25µm	525$\pm$25µm

Table 6: Thickness of layers in different batches of test structures

Current-voltage characterization was performed on the type A structures and the resistance value at 50mV was plotted. The resistance values for 25 different structures were plotted for each batch on five different dies were used for plotting histograms. Histograms were used to analyse the different resistance prior to radiation. The histograms for batch 1 and batch 2 have been plotted in figures 20 and 21 respectively.

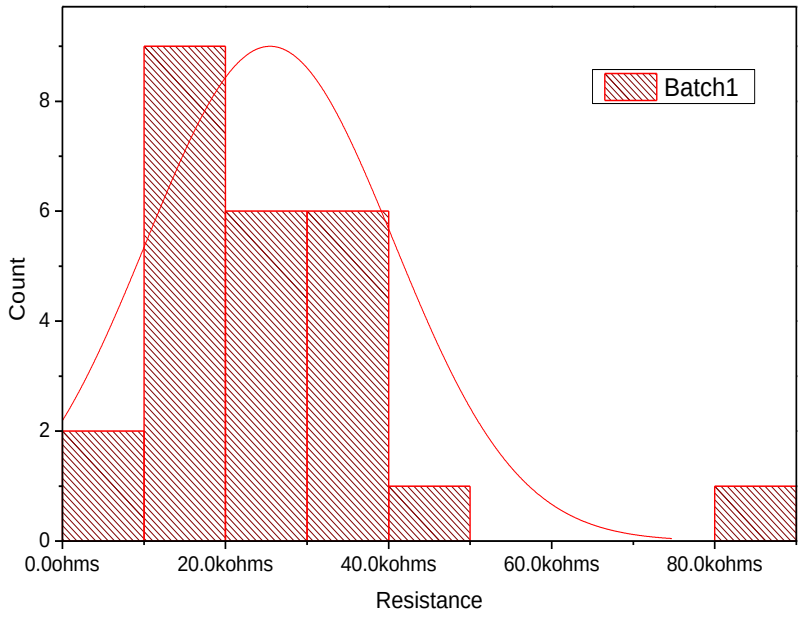

Figure 20: Histogram of pre-irradiation resistance level for batch1

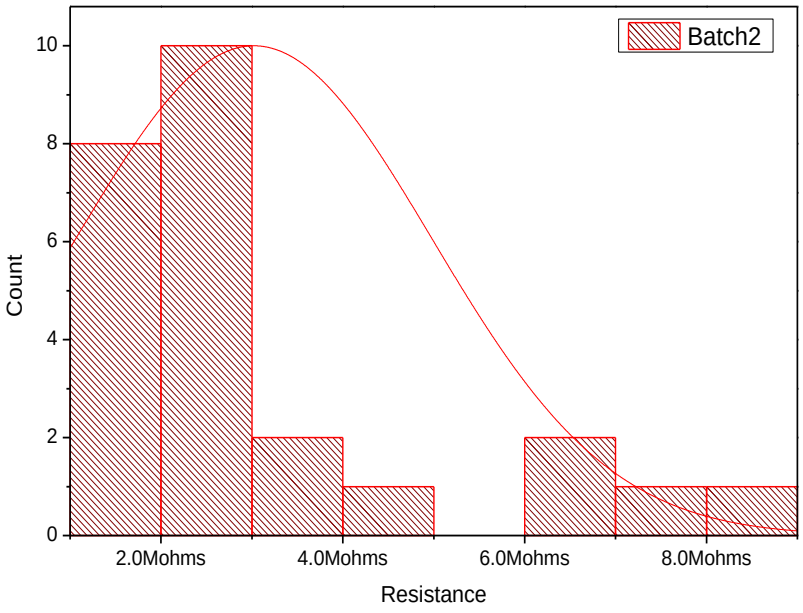

Figure 21: Histogram of pre-irradiation resistance level for batch2

A lower mean resistance value of 25.4 KΩ is observed in the case of batch 1 structures compared to batch 2 which has a mean resistance value of 2.04MΩ.It is also observed that the distribution is not centred around the mean and there are samples lying beyond the tail. This may be due to the variation within a wafer from die to die due to change in thicknesses across the wafer. A thicker layer of silver (60 nm) suggests that the structure has a lower resistance level when compared to thinner silver(35-40 nm). This can be explained as the roughness of the film increases as we decrease thickness of the film. Thicker films have lesser agglomeration compared to thinner films. This reduces the thickness of silver at the top and interface between both the layers moves into the ChG reducing the integrity of the film. The thicker silver results in more silver on top of the ChG and less rougher films. Studies have been reported with impact of thickness of silver on silicon-dioxide layers suggesting similar results [15].

The thickness of batch1 and batch 2 structures were confirmed using transmission electron microscopy (TEM) images. Figure 22 and 23 are the TEM images of the cross-section for batch 1 and batch 2 structures.

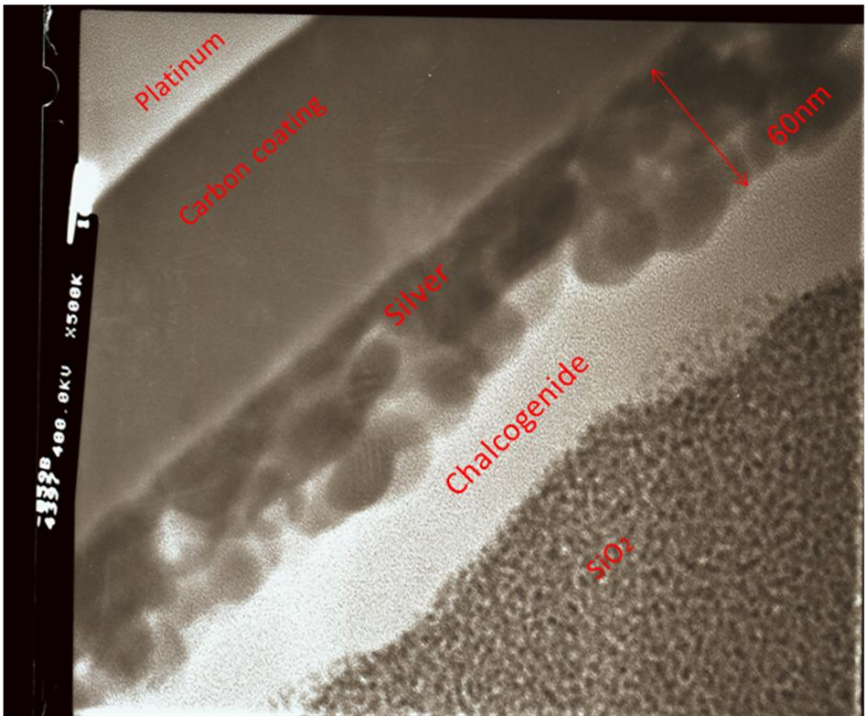

Figure 22: TEM image of the cross-section of batch1 type A structure.

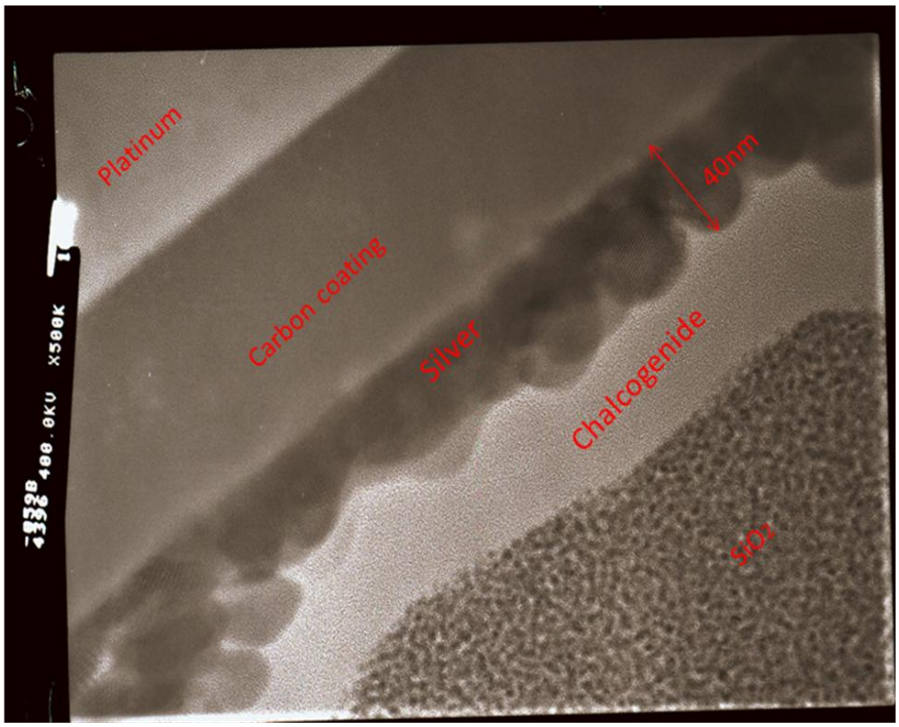

Figure 23: TEM image of the cross-section of batch2 type A structure

The images were taken by CSSS staff at leroy eyring centre at arizona state university. The thickness of silver layers was confirmed with the images for control structures. It can also be noticed that silver has been incorporated into the ChG layer confirming the diffusion of silver which takes place at room temperature.

3.5.1 Impact of thickness on sensing parameters

The output (resistance) was plotted for structures from batch 1 and batch 2 for radiation dose of 800 k rad as shown in figure 24. It was noticed that for both the batches change in dose/ dB is close to 400 k rad. This suggests that both the batches have similar sensitivity independent of the thickness of silver.

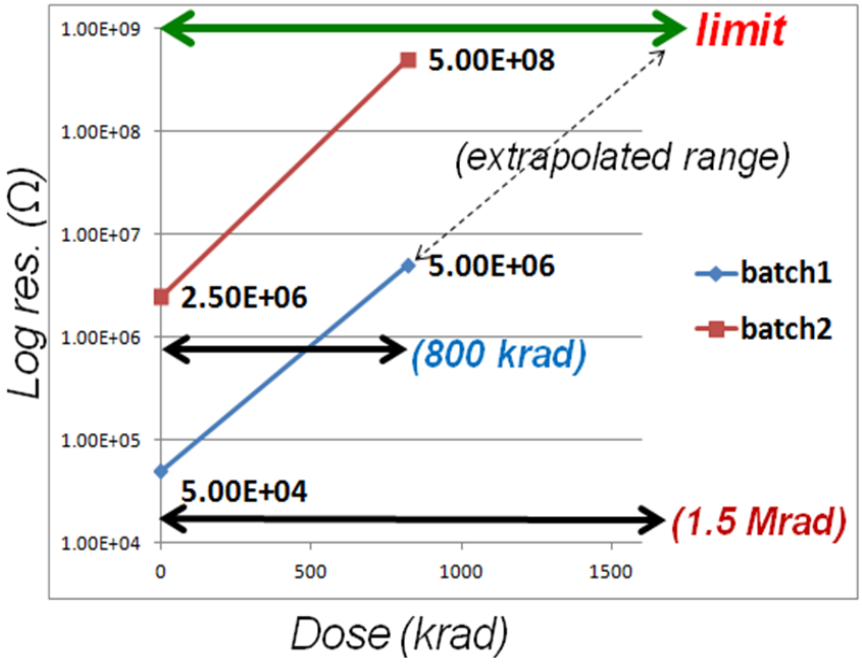

Figure 24: Resistance plotted as a function of dose for batch1and 2

It can also be seen from figure 24 that in the case of batch 1 with lower pre-irradiation resistance level, there is an extended range of operation for the sensor. The range is limited in the case batch2 at 800k rad. The limit is set by the maximum resistance that can be measured with the instrument.

4 Energy dispersive spectroscopy (EDS) on test structures

EDS is a material analysis technique used for elemental analysis and chemical characterization of the sample. The fundamental principle behind the technique is that each element has a unique atomic structure which corresponds to a unique set of peaks on the energy spectrum. EDS was carried out on the test structures at Boise State University facility by Dr Maria Mitkova's group on the test structures. The results from the analysis have been summarized.

EDS provides an average elemental composition of all the material within the area up to a depth of 1 µm. The inter digitiated fingers were used for this characterization as they have smaller finger spacing between them (20µm) and have parallel fingers similar to type A structures. Area scans were made over the sample along the lines as shown in figure 25 and 26. Area scans were preferred as they are less damaging to the films in comparison to point scans which results in silver moving during the measurement. This can affect the accuracy of the composition of the material.

The percentage of Ag, Ge and Se ternary were calculated using the following equation:

Ge%= (100)*(Ge%/(Ge%+Se%+Ag%))

Se%= (100)*(Se%/(Ge%+Se%+Ag%))

Ag%= (100)*(Ag%/(Ge%+Se%+Ag%))

The values shown on the SEM image in figure 26 and 26 correspond to Ag% as a part of the GeSeAg analysis.

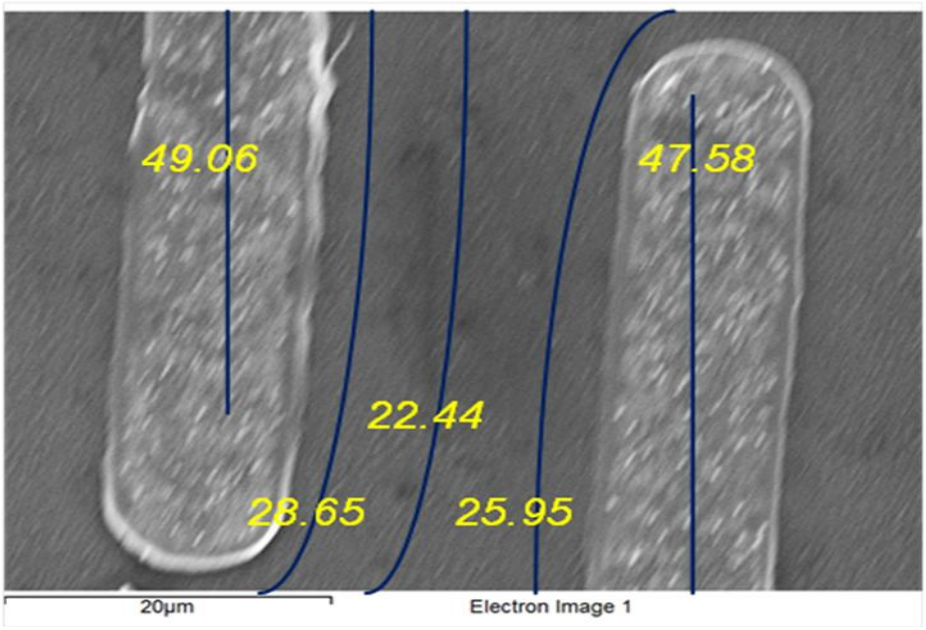

Figure 25 : SEM image of control sample

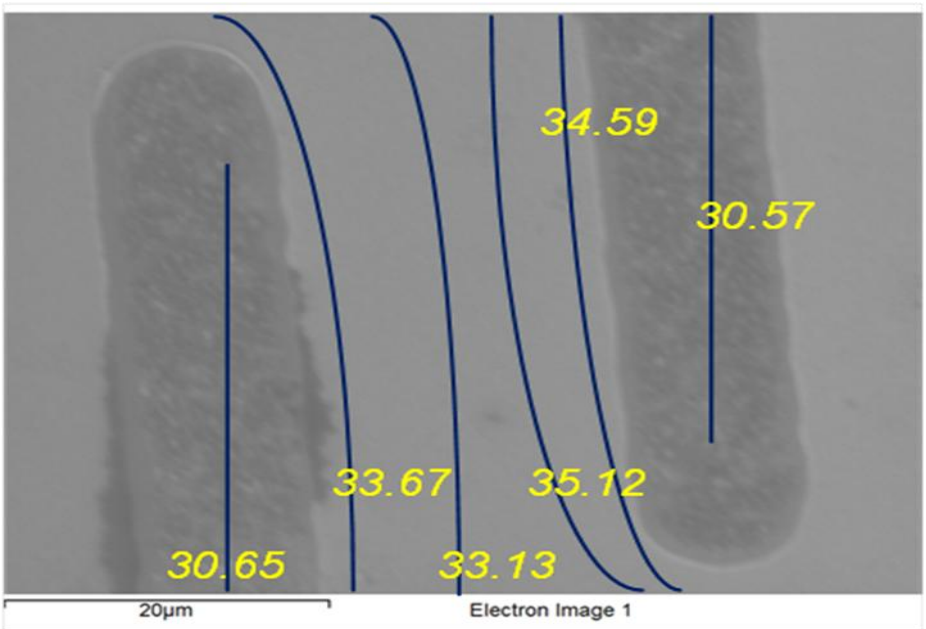

Figure 26: SEM image of irradiated sample

The Ag concentration was plotted as a function of distance (from Ni fingers) in figure 27.

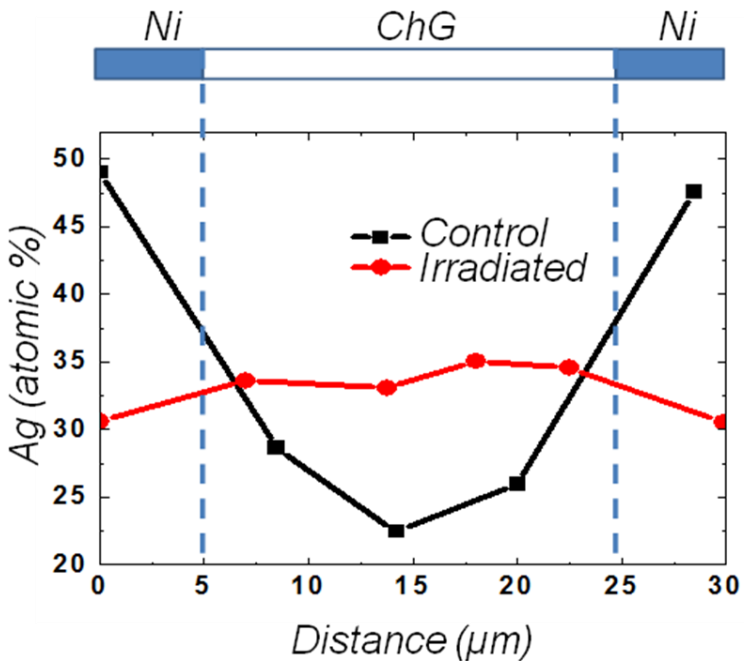

Figure 27: Ag distribution as function of distance

It can be seen from figure 27 that we have a higher concentration of silver below the nickel pads prior to irradiation. This could be due to a higher work potential of nickel which causes the silver to stay close to the nickel edge or the processing conditions which attracts silver. When the samples are irradiated, the concentration distribution is more uniform with mild variations.

5 Atomic Force Microscopy (AFM) Characterization of the test structures

5.1 Atomic Force Microscopy

AFM is a material characterization technique used to analyse surface of the sample by scanning a tip over the sample. The force between the tip and the sample is measured. The tip is attached to the cantilever which deflects the laser beam incident on it depending on the forces (attractive or repulsive) between the sample and the tip. The deflections are monitored using a photodiode and an image of the surface is generated. AFM can be operated in three modes depending on the application-contact, non contact and tapping (intermittent) mode [16]. The resolution of AFM ranges from 1-20nm depending on the sharpness of the tip.

5.2 Surface analysis of test structures

AFM was used to analysis the surface of the test structures. Tapping mode AFM was chosen to the study the topography of the lateral test structures. This mode was chosen as it provides high resolution images without causing damage to the surface of the sample [17]. AFM method was chosen to study these test structures as the resistance value of the materials was found to be sensitive to radiation (U.V and gamma). The roughness of the silver and germanium selenide will be analysed to post and prior to irradiation. Dendrites were present on the control sample prior to radiation and their dissolution after radiation was investigated using AFM.

Agilent scanning probe microscopy (SPM) dimension was operated in tapping mode to make scans over the sample surface. The scans were concentrated on four

regions as shown in the figure 28. Region A is the nickel, silver and germanium selenide lateral interface. Region B is the silver and germanium selenide lateral interface on regions where there is no nickel electrode on top. Region C scans the silver surface over the region where there is no nickel on top. Region D scans the chalcogenide surface.

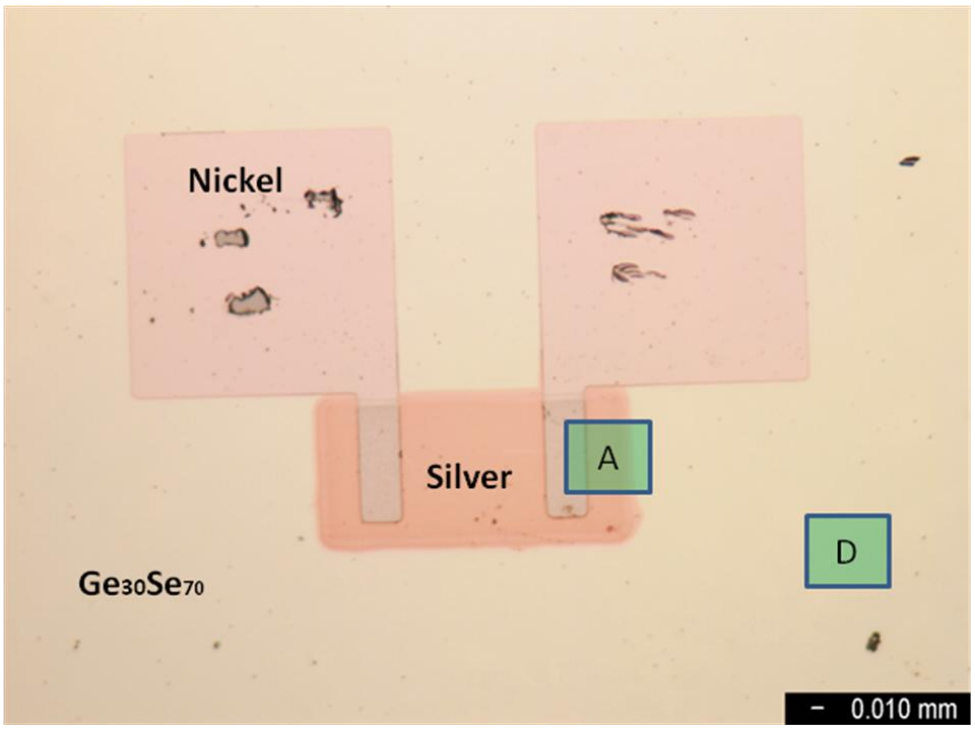

(a)

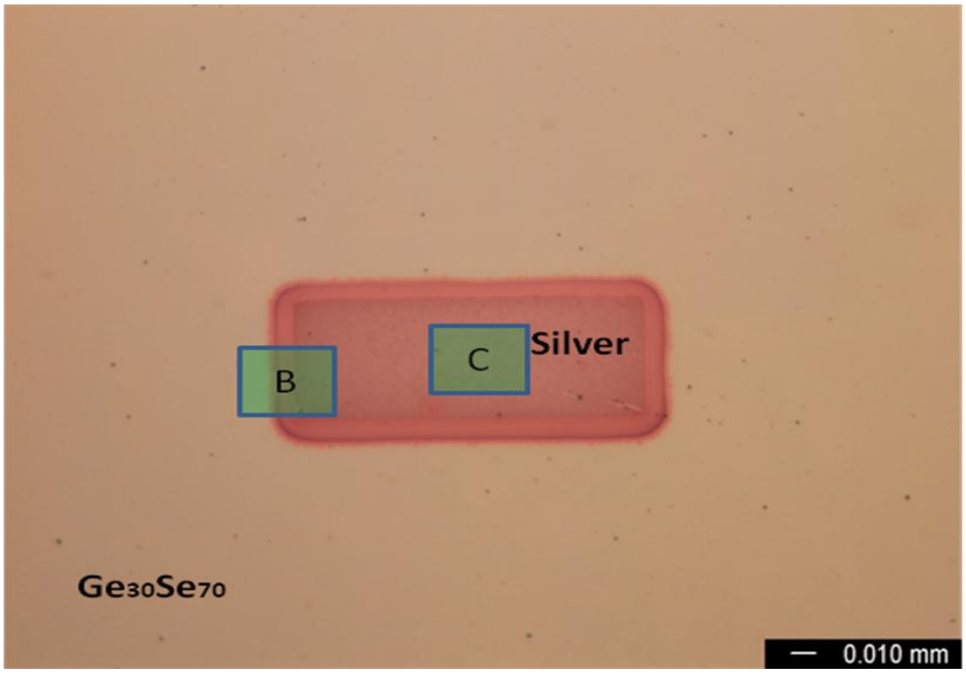

(b)

Figure 28: AFM scans over the test structure

A new batch of test structures were fabricated to perform AFM characterization on them and to check the effect of UV and Gamma on the test structures. These devices were manufactured keeping the same thickness as the previous batch; however there will be changes in thickness owing to difference in small processing parameters.

The AFM scans were carried out with minimal light but light used for focussing the surface could not be avoided. This may impact the silver and chalcogenide system as both chalcogenide and silver are sensitive to light. The AFM images were analysed using Nanoscope software package which is used along with bruker SPM. The image was flattened and plane fitted before any depth or

roughness analysis [18]. Roughness command generated statistical values depending on the height of each pixel in the image. Plane fitting applies a temporary first-order plane fit before calculating statistics. On many surfaces, especially those which are tilted, this yields different values from those seen in raw (un-plane fitted) data. Flattening the image avoids bow in images.

5.2.1 Region A scan (Nickel-Silver-Chg edge)

A 50µm scan was made over this region and the scan speed was set to 1.2Hz with slow scan axis enabled. The AFM image of region A for the Control, Gamma irradiated and UV exposed test structures were taken. Region A scan indicates if there is any change in dimensions of the silver region after it has been prior and post irradiation. The step profile of the surface has been shown in figure 29 for control and irradiated die.

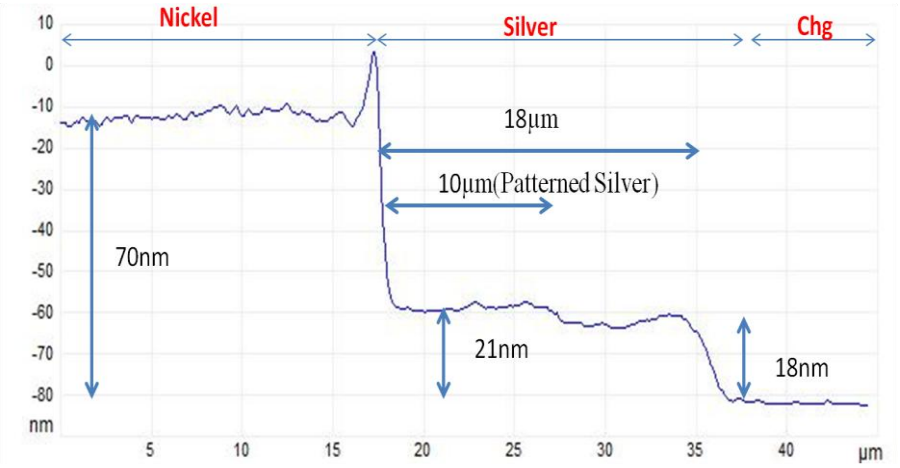

(a)

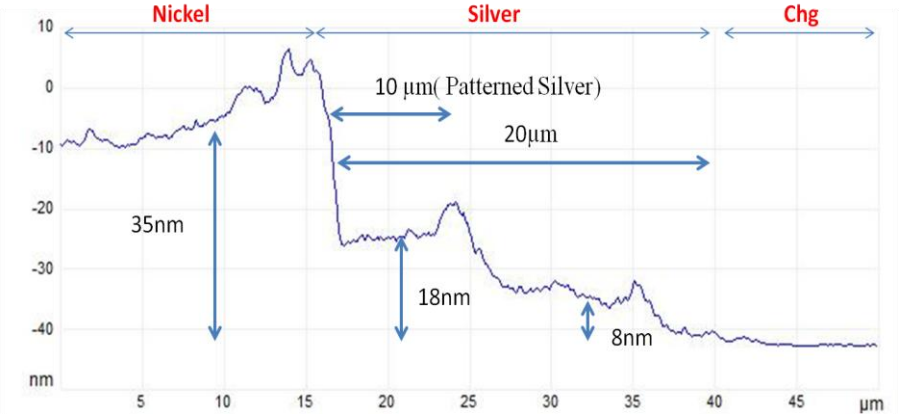

(b)

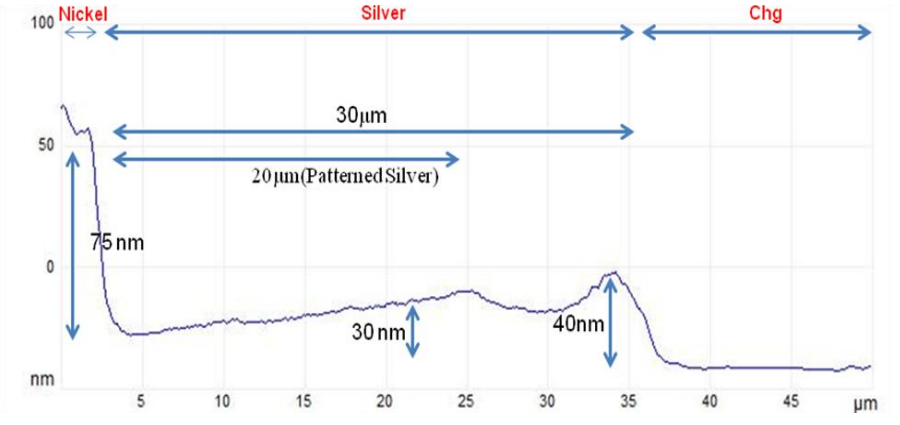

(c)

Figure 29: Topography analysis of the Test structures along the Nickel finger; Step profile for control (a),U.V exposed (b) and Gamma irradiated (c) structures

It is observed that there is a change in diffusion length with UV exposure. There is no change in length with Gamma irradiation until 400 Krad. This difference may be due to the fact that the dose to which the test structure was exposed in the case of UV is much larger in magnitude when compared to Gamma dose when they are compared in terms of energy the test structure is exposed. The step which is present between the chalcogenide and the patterned silver is evened out after exposure both in the case of UV and Gamma as shown in the figure

5.2.2 Region B Scan- Silver-Chg edge

A 30µm scan was made over this region and the scan speed was set to 1.2Hz with slow scan axis enabled. The AFM image of region A for the Control, Gamma irradiated and UV exposed test structures were taken as shown in figure 30. Region B scan indicates if there is any change in roughness of the silver surface and if there is dissolution of dendrites prior to and post irradiation. The dimensions of the silver region can also be checked.

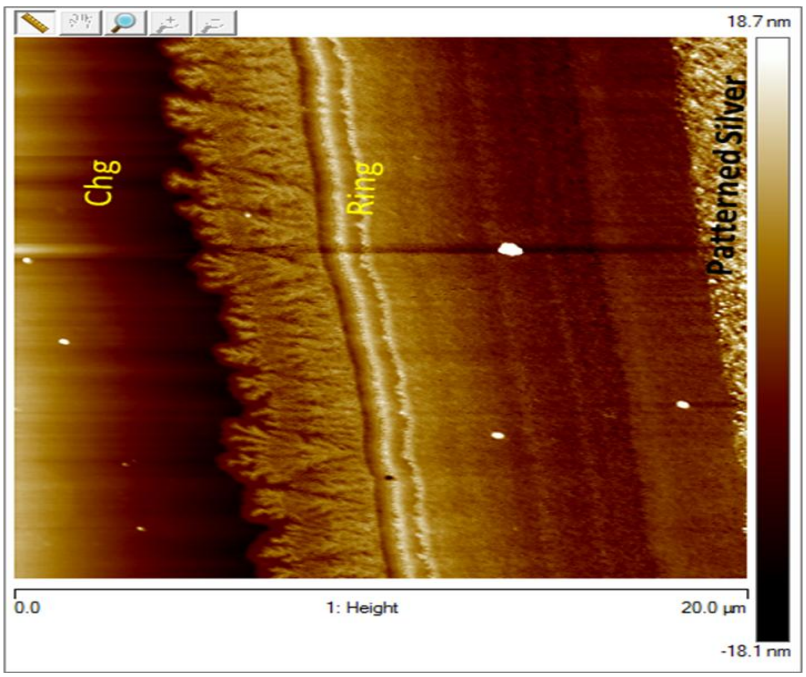
18.7 nm
Chg
Ring
Patterned Silver
0.0
1: Height
20.0 µm
-18.1 nm

(a)

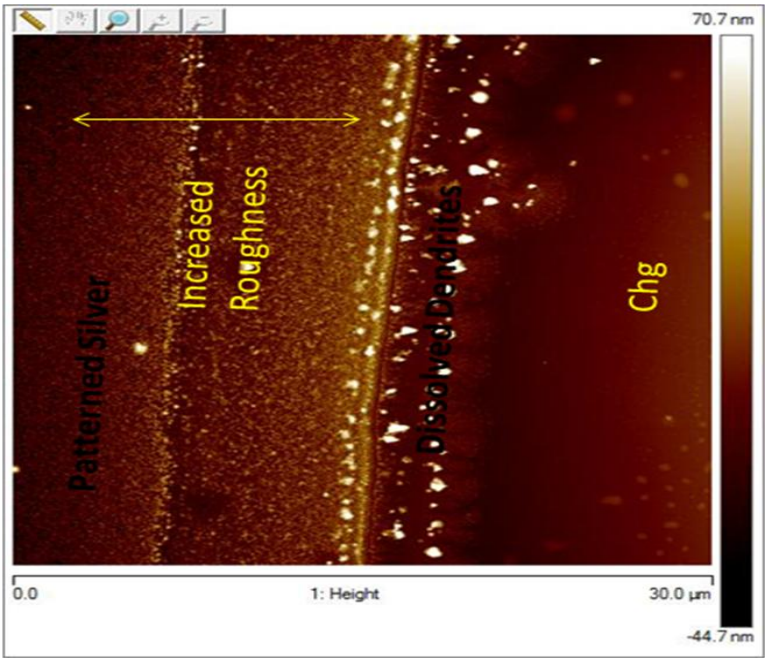
70.7 nm
Patterned Silver
Increased
Roughness
Dissolved Dendrites
Chg
0.0
1: Height
30.0 µm
-44.7 nm

(b)

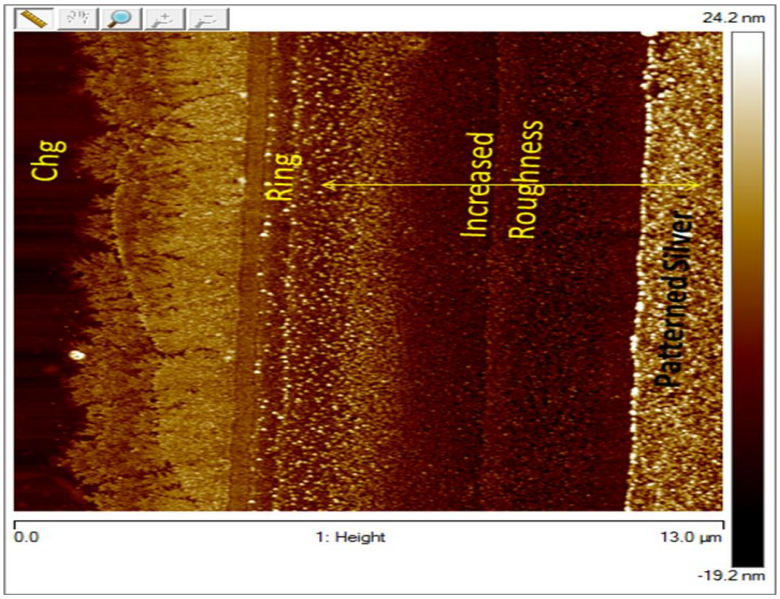

(c)

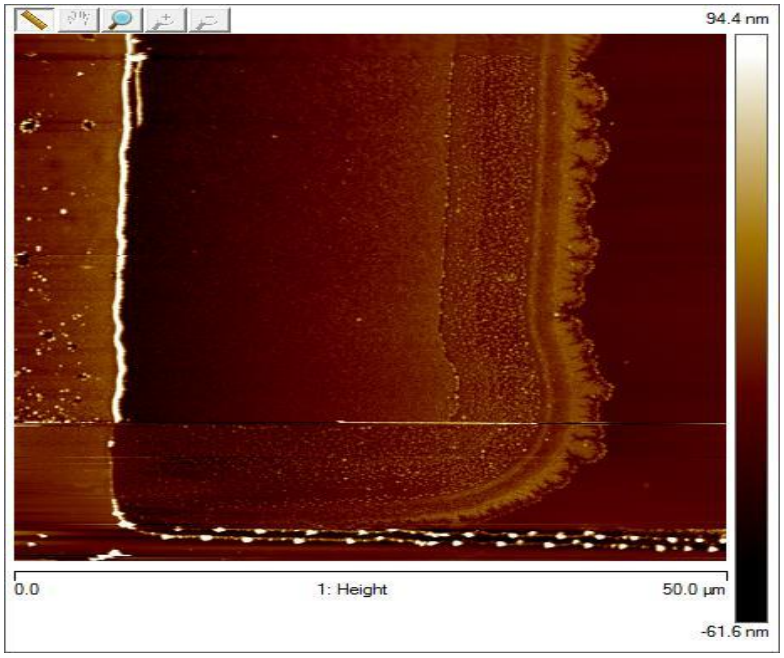

(d)

Figure 30: AFM Image of the Silver and chalcogenide interface; Scans were made for control (a), UV exposed (b) gamma irradiated (c) annealed (d) die

The roughness analysis on this region indicates that there is an increase in silver roughness with exposure. This suggests that we have more silver being incorporated into the chalcogenide. The dendrites which appear along the edge of the silver pad become lighter in contrast indicating that the silver from the dendrites have been incorporated into the chalcogenide film. There is always a ring along the silver edge which is formed at room temperature; this is an area of lesser roughness compared to the region of silver close to the nickel (where the silver is originally patterned). It is seen that both roughness of the patterned and ring region increases after exposure.

An AFM scan was also made on a test structure which was kept at room temperature after being irradiated and it was noticed that dendrites [19] re-appeared along the edge of the silver. This suggests that we have photo stimulated deposition of silver taking place at room temperature. This accounts for the recovery of resistance level to pre-irradiation level and lower values as seen with the electrical results.

5.2.3 Region C scan- silver

A 5μm scan was made over this region and the scan speed was set to 1.2 Hz with slow scan axis enabled. The AFM image of region C for the control, gamma irradiated and UV exposed test structures were taken as shown in figure 31. Region C scan indicates if there is any change in roughness of the silver surface prior to and post irradiation. This scan was taken to concentrate on the patterned part of the silver alone and check the difference brought about in roughness.

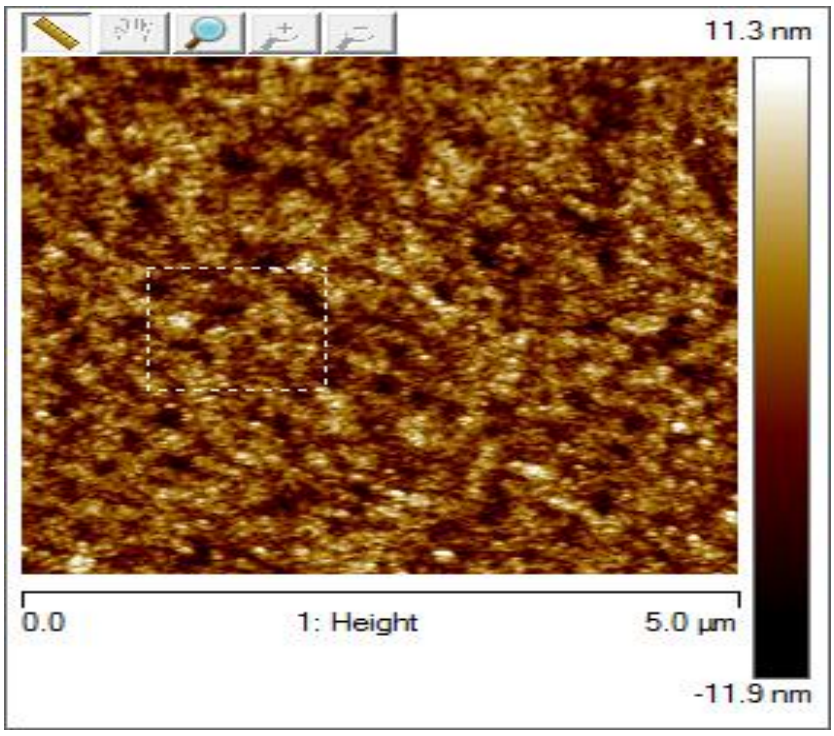

(a)

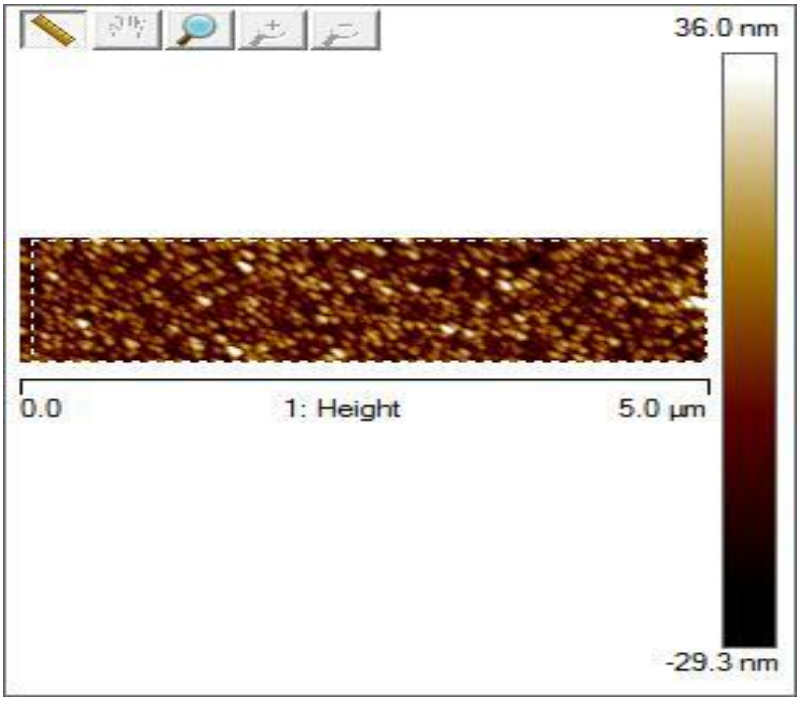

(b)

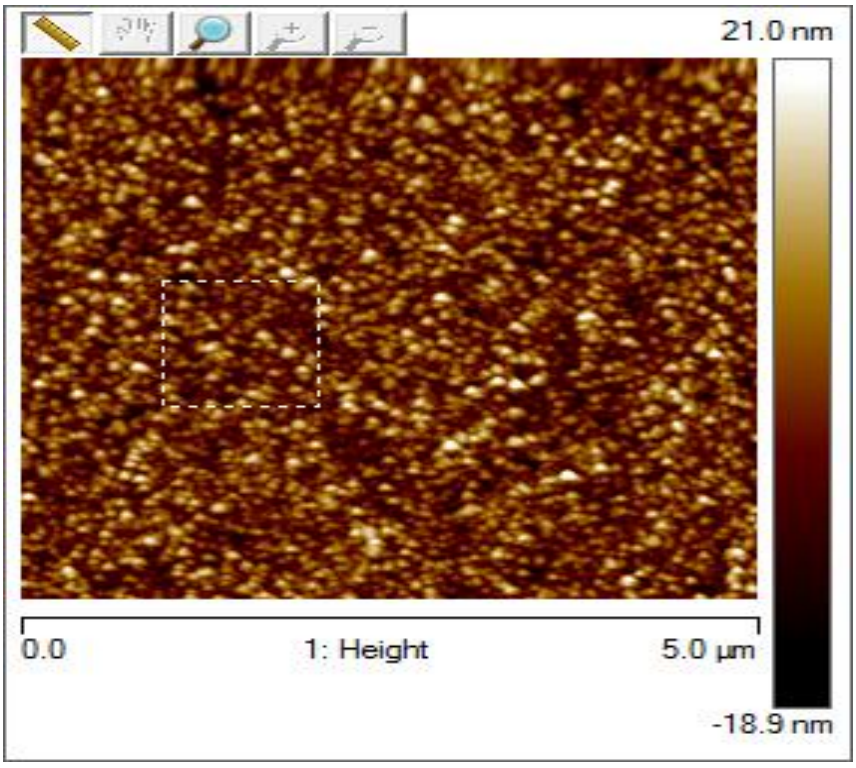

(c)

Figure 31: AFM scan over the Silver region; Scans were made for Control(a), UV exposed (b) and Gamma irradiated (c) die

The roughness of the silver films prior to irradiation was close to 25 nm. This indicates that the film is not continuous prior to irradiation which corresponds to a high resistance pre-irradiation level electrically. A smooth continuous film has a roughness close to 3-4 nm. The roughness of the film increases further on exposure to radiation. This increase in roughness corresponds to 25nm. This suggests that there is a further loss in continuity of the film with radiation which corresponds to a further increase in resistance electrically.

5.2.4 Region D scan- chalcogenide

A 5µm scan was made over this region and the scan speed was set to 1.2Hz with slow scan axis enabled. The AFM image of region D for the Control, Gamma irradiated and UV exposed test structures were taken as shown in figure 32. Region D scan indicates if there is any change in roughness of the chalcogenide surface prior to and post irradiation.

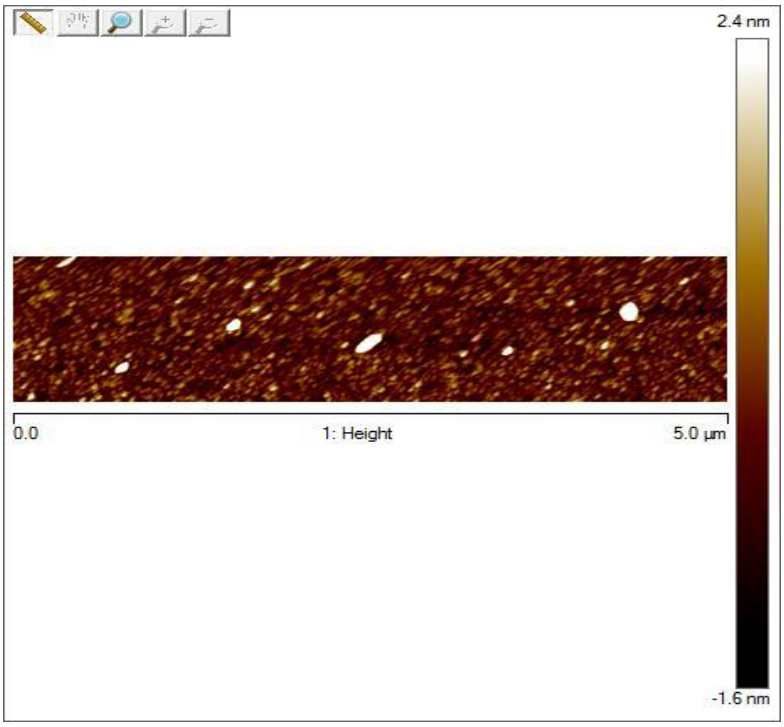

Figure 32: AFM scan over the chalcogenide region .

This scan was taken to concentrate on the chalcogenide alone and check the difference brought about in roughness of the film. There is no change in roughness of the film and they continue to remain smooth after exposure to both UV and gamma.

6 Summary and outlook

It has been experimentally observed that there is a change in resistance of the test structures when irradiated. The initial resistance of the test structure prior to irradiation is lower compared to the value of resistance obtained post irradiation. The initial value of resistance obtained is high compared to the resistivity of silver films due to processing steps and agglomeration of thin silver films. The initial value of resistance depends on various parameters such as the thickness of the silver film, the thickness of chalcogenide film and the saturation level of the films and rate at which silver film is deposited on the chalcogenide film. The deposition rate is kept low to ensure there is minimal diffusion of silver while the film is being deposited. A higher thickness of silver can result in higher values of resistance as this prevents the silver film from agglomerating on the surface. It should be kept in mind that at higher thicknesses of silver, the transparency of the film reduces.

The increase in resistance upon exposure to U.V and gamma radiation was understood using AFM material characterisation technique. It was noticed that the change in resistance was brought about only when the test structure was irradiated continuously at once to a certain dose. There is no change in resistance observed at smaller dose steps suggesting a possibility of certain threshold value of dose required for dissolution of silver into the chalcogenide film. The dissolution of silver into the film is indicated by the difference in roughness of the films as studied using AFM material characterisation. Dendrites are observed along the

edge of the silver pad and their dissolution upon irradiation can be understood with the help of AFM. The dissolution of dendrites is a function of the radiation dose and takes place only at a certain threshold of radiation dose. Annealing behaviour is also noticed in these test structures; the test structures recover their value of resistance once they are removed from the irradiation chamber and stored at room temperature. This recovery was explained with photo-stimulated deposition of silver at room temperature.AFM confirms the reappearance of dendrites on the ChG surface along the silver edge suggesting photo-stimulated deposition process. A re-exposure was performed after room temperature annealing of the test structures using UV light and the same behaviour was noticed as before- an increase in resistance on exposure and recovery of the initial lower resistance level when left at room temperature. This indicates that these test structures are sensitive even after they have recovered from a previous exposure.

The initial pre-irradiation resistance level was found to be a function of the silver thickness. A thicker silver corresponds to a lesser agglomerated film with lower resistance, thereby increasing the range of operation of the sensor.

It was experimentally proven that there is a change in resistance of these test structures with radiation dose. This shows that the silver incorporation into the chalcogenide films is sensitive to radiation dose. These materials can be used to build radiation sensors. It has also been noticed that there is a certain threshold of radiation dose before which we see a change in resistance; this can be useful in making sensors that are specific to dose level. The sensitivity of the test structures

to the dose magnitude has to be further investigated to build structures that can be made sensitive to specific dose values.

REFERENCES

[1] [Online].*Radiation sensors.* Retrieved from http://www.blackcatsystems.com/GM/RadiationSensor.html

[2] [Online].*Intelligent radiation sensing.* Retrieved from http://www.dhs.gov/intelligent-radiation-sensing-system

[3] [Online].*Sensors fundamentals.* Retrieved from http://www.ni.com/white-paper/4045/en

[4] Kolobov, A. V., & Elliott, S. R. (1991). Photodoping of amorphous chalcogenides by metals. *Advances in Physics, 40*(5), 625-684. doi: 10.1080/00018739100101532

[5] Wagner, T. (2002). Photo-and thermally-induced diffusion and dissolution of Ag in chalcogenide glasses thin films. *Journal of Optoelectronics and Advanced Materials*, *4*(3),717-727.

[6] Mitkova, M., & Kozicki, M. N. (2002). Silver incorporation in Ge–Se glasses used in programmable metallization cell devices. *Journal of non-crystalline solids*, *299*, 1023-1027.

[7] Mitkova, M., Kozicki, M. N., Kim, H. C., & Alford, T. L. (2004). Local structure resulting from photo and thermal diffusion of Ag in Ge–Se thin films. *Journal of non-crystalline solids*, *338*, 552-556.

[8] Kozicki, M. N., Park, M., & Mitkova, M. (2005). Nanoscale memory elements based on solid-state electrolytes. *Nanotechnology, IEEE Transactions on*, *4*(3), 331-338.

[9] Kozicki, M. N., Mitkova, M., Park, M., Balakrishnan, M., & Gopalan, C. (2003). Information storage using nanoscale electrodeposition of metal in solid electrolytes. *Superlattices and Microstructures, 34*(3–6), 459-465. doi: 10.1016/j.spmi.2004.03.042

[10] Valov, I., Waser, R., Jameson, J. R., & Kozicki, M. N. (2011). Electrochemical metallization memories—fundamentals, applications, prospects. *Nanotechnology, 22*(25), 254003.

[11] Kozicki, M. N., & Mitkova, M. (2006). Mass transport in chalcogenide electrolyte films – materials and applications. *Journal of Non-Crystalline Solids, 352*(6–7), 567-577. doi: 10.1016/j.jnoncrysol.2005.11.065

[12] Mitkova, M., & Kozicki, M. N. (2002). Silver incorporation in Ge–Se glasses used in programmable metallization cell devices. *Journal of Non-Crystalline Solids, 299–302, Part 2*(0), 1023-1027. doi: 10.1016/S0022-3093(01)01068-7

[13] Kawaguchi, Takeshi; Maruno, Shigeo; , "Photoinduced surface deposition of metallic silver in Ag-As-S glasses," *Journal of Applied Physics* , vol.77, no.2, pp.628-634, Jan 1995 doi: 10.1063/1.359048

[14] Kawaguchi, T., Maruno, S., & Elliott, S. R. (1997). Compositional dependence of the photoinduced surface deposition of metallic silver in Ag□ As□ S glasses.*Journal of non-crystalline solids*, *211*(1), 187-195.

[15] Kim, H., Alford, T., & Allee, D. (2002). Thickness dependence on the thermal stability of silver thin films. *Applied Physics Letters*, *81*(22), 4287-4289.

[16] Chen, C. J. (1993). *Introduction to scanning tunneling microscopy* Oxford University Press, USA.

[17] Rugar, D., & Hansma, P. (1990). Atomic force microscopy. *Phys.Today*, *43*(10), 23-30

[18] [Online].*Nanoscope analysis.* Retrieved from http://nanoscaleworld.bruker-axs.com/nanoscaleworld/media/p/775.aspx

[19] Mitkova, M. I., Kozicki, M. N., & Aberouette, J. P. (2003). Morphology of electrochemically grown silver deposits on silver-saturated Ge–Se thin films.*Journal of non-crystalline solids*, *326*, 425-429.

.